An Improved Switching Method-Based Diagnostic Strategy for IGBT Open-Circuit Faults in Hybrid Modular Multilevel Converters

Hong Wu, *Student Member, IEEE*, Yue Wang, *Senior Member, IEEE*, Yi Liu, *Student Member, IEEE*, Yonghui Liu, *Member, IEEE*, and Yufei Li, *Senior Member, IEEE*

***Abstract*—The hybrid modular multilevel converter (HMMC) has attracted extensive attention due to its dc fault ride-through capability. However, the research on its insulated gate bipolar transistor (IGBT) open-circuit fault (OCF) diagnosis is still barely seen, which becomes a research gap that may jeopardize the reliability of the HMMC system. To address this issue, this article first proposes an improved switching method, which can ensure all six types of IGBT OCFs unveil their fault characteristics thoroughly by using an extra bypassed switching sequence. Furthermore, the improved switching method remains the same switching loss as the existing switching method. Afterward, a diagnostic method is brought forward to identify the faulty SM by its fixed specific sequence in a period of time while the switching sequences of other SMs with the same type are dynamic. On this basis, an improved switching method-based diagnostic strategy that consists of various types of diagnostic methods is proposed, which can diagnose all six types of IGBT OCFs in the HMMC within 20 ms and have immunity to dc faults and load change. Experimental results in a hardware-in-the-loop platform verify the effectiveness of the proposed switching method and diagnostic strategy.**

***Index Terms*—Diagnostic strategy, hybrid modular multilevel converters, open-circuit fault, switching loss, switching method.**

NOMENCLATURE

N	Number of SMs in each arm.
L	Arm inductor.
$U_{\rm dc}$, $I_{\rm dc}$	DC voltage, current.
j	Phase j.
u, l	u: upper arm, l: lower arm.
i	Sequence number of SM.
u_{Ci}	Capacitor voltage of SM.
$U_{{\rm sm}i}$	Output voltage of SM.
S_i	Switching sequence of SM.
$S_{\text{Fun-}i}$	Switching function of SM.
$M_{\rm ac}$	AC modulation index.
$U_{\rm m}$	Amplitude of the output ac voltage.
$U_{\rm dcn}$	Rated dc voltage.
$M_{\rm dc}$	DC modulation index.
$N_{\rm on}$	Number of inserted SMs.
F_i	Bypassed switching sequence selection flag.
$I_{\rm flag}$	Initial flag.
B	Set of SMs whose switching sequence remains in a same value.
A	Set of SMs whose switching sequence equals to a same value.
$N_{\rm sw}$	Number of SMs whose switching sequence switches from a same value.
$N_{\text{sw-sum}}$	Sum of $N_{\rm sw}$s during several control periods.
$N_{\rm th}$	Diagnostic threshold.
$E_{\rm on}$	Turn-ON loss of IGBT.
$E_{\rm off}$	Turn-OFF loss of IGBT.
$E_{\rm rec}$	Reverse recovery loss of diode.
$E_{\rm pro}$	Switching loss of the proposed switching method.
$E_{\rm exi}$	Switching loss of the existing switching method.
$f_{\rm sw}$	IGBT switching frequency.
$N_{\rm FT}$	Faulty type of faulty SM.
$N_{\rm FN}$	Sequence number of faulty SM.

Received 1 February 2024; revised 9 June 2024 and 26 September 2024; accepted 31 October 2024. Date of publication 6 November 2024; date of current version 18 December 2024. This work was supported in part by the National Key R&D Program of China under Grant 2023YFB2406700 and in part by the Science and Technology Projects of State Grid Corporation of China under Grant J2023001. Recommended for publication by Associate Editor M. Liserre. *(Corresponding authors: Yue Wang; Yufei Li.)*

The authors are with the State Key Laboratory of Electrical Insulation and Power Equipment, Xi'an Jiaotong University, Xi'an 710049, China (e-mail: wuhong30@stu.xjtu.edu.cn; davidwangyue@mail.xjtu.edu.cn; 4121104089@stu.xjtu.edu.cn; yh.liu@xjtu.edu.cn; yfliee@xjtu.edu.cn).

Color versions of one or more figures in this article are available at https://doi.org/10.1109/TPEL.2024.3492236.

Digital Object Identifier 10.1109/TPEL.2024.3492236

I. INTRODUCTION

THE modular multilevel converters (MMCs) feature modular structure and excellent scalability, which is regarded as the most promising converter in high-voltage scenarios, especially in flexible-high voltage direct current (Flexible-HVDC) [1], [2], [3]. The most common submodule (SM) in an MMC is the half-bridge submodule (HBSM), which contributes to the lowest number of power devices and costs [4]. However, the half-bridge MMC (HBMMC) does not have dc fault ride-through capability due to anti-parallel diodes equipped in IGBTs [5]. The full-bridge submodule (FBSM) stands out as a perfect solution for dc fault ride-through capability among all other novel SM topologies proposed by both academia and industry [6], [7], [8]. Unfortunately, the cost of full-bridge MMC (FBMMC) is much higher than that of HBMMC because of the doubled number of power devices [9]. The hybrid MMC (HMMC) is proposed in [10], which combines the advantages of both HBMMCs and FBMMCs. The HMMCs comprise both

FBSMs and HBSMs, which have been applied in the Wudongde Flexible-HVDC Project in Southwestern China [11]. As the number of SMs increases, the number of potential failure points also increases correspondingly, which becomes severer when it comes to HMMCs since they consist of more power devices than the HBMMCs do [12]. Therefore, the reliability of the HMMC deserves further investigation.

The power device, such as the insulated gate bipolar transistor (IGBT) is one of the key components that affect the reliability of HMMCs [13]. The fault of an IGBT can be classified into two types: short-circuit faults (SCFs) and open-circuit faults (OCFs) [14]. The SCFs are extremely destructive and some well-established diagnostic strategies have been proposed to address them [15]. On the contrary, the OCFs may not be as destructive as the SCFs immediately but can jeopardize the normal operation of MMCs later, and even cause further faults in other normal components [16]. Moreover, the complicated fault characteristics of IGBT OCFs also complicate their diagnoses. Hence, this article mainly focuses on the diagnosis of IGBT OCFs.

Over the past few years, several IGBT OCF diagnostic strategies have been proposed. However, most of them only consider the cases in HBMMCs. For instance, strategies in [17] and [18] rely on the hardware to diagnose faults. A hardware circuit-based on a rearranged bleeding resistor is proposed to diagnose IGBT OCFs for HBMMCs under light load [17]. In [18], the objects of the voltage sensors are changed from the SM capacitor voltage to the SM output voltage by adjusting the installation locations. However, the extra hardware circuits increase cost and bring in more potential failure points. Moreover, the adjustment of the installation locations is still not permitted for commercial MMCs. To avoid reliance on hardware, strategies in [19], [20], and [21] use artificial intelligence (AI) algorithms to diagnose faults. In [19], binary neural networks are employed for diagnosis, which entails a slight reduction in accuracy but a significant reduction in storage space. A sliding-time window is used to record data of the operating parameters in the HBMMC and then the data are used to train a two-dimensional convolutional neural network (2-D CNN) [20]. Then, the OCF can be easily diagnosed with the trained 2-D CNN. In [21], it proposes a diagnostic strategy that can still work correctly in the presence of missing data and severe noise, whose diagnostic process is conducted through an extreme gradient boosting algorithm. These diagnostic strategies based on AI algorithms do not rely on hardware-circuit revamps but usually suffer from tremendous computational burdens. Thus, the requirement of enhancing the computational power of industrial controllers limits these strategies' further applications. Except for the strategies based on hardware circuits or AI algorithms, there exists another type of diagnostic strategy based on system models. In [22], it first constructs a matrix that consists of SM capacitor voltages and uses the single-ring-theorem as a mathematical tool to analyze the matrix for fault detection. The malfunctioning SMs can be further located using a boxplot. In [23], the proposed strategy first obtains the number and the type of malfunctioning SMs by comparing the measured value of the arm voltage with its estimated value. Then, the specific malfunctioning SMs can be confirmed rapidly by virtual capacitor voltages. A repetitive signal generator is used to judge the periodicity of the capacitor voltage deviations, then the malfunctioning arm can be confirmed [24].

All the above diagnostic strategies target at HBMMCs. The strategies in [25] and [26] consider the cases in FBMMCs. However, paper [25] only considers the case under the carrier phase shift pulsewidth modulation but ignores the case under the nearest level modulation (NLM), which is more widely used in high power-level scenarios. Although paper [26] considers the case under the NLM, it is forced to ignore some malfunctioning types due to the limitations of the existing switching method [26]. Compared with HBMMCs and FBMMCs, HMMCs have more types of IGBT OCFs, more complex fault characteristics, and greater difficulties in their diagnosis due to the co-existence of HBSMs and FBSMs, which also renders the existing diagnostic strategies unable to be used in HMMCs directly. Consequently, there is still a research gap in the diagnostic strategies of IGBT OCFs in HMMCs. Therefore, it is necessary to conduct in-depth research on IGBT OCF diagnosis in HMMCs to guarantee its reliability.

Toward this end, an improved switching method that complements the missing operating modes of the existing switching method by adding a bypassed switching sequence is proposed. Through the analysis of fault characteristics under two switching methods, it is demonstrated that the proposed switching method can ensure all types of IGBT OCFs reveal their fault characteristics thoroughly, while certain characteristics are missing in the existing switching method. Then, it is shown that all six types of malfunctioning SMs remain in specific switching sequences in the corresponding parts while the switching sequences of normal SMs with the same type in the HMMC are all in dynamic change in most cases or all remain at a specific value at special case (the parts are divided by the polarity of the arm current and the number of inserted SMs). Based on this feature, a diagnostic method is proposed to identify the SM with the fixed specific sequence in a period of time while the switching sequence of other SMs with the same type is still dynamically changing. Further, an improved switching method-based diagnostic strategy for IGBT OCFs in HMMCs consisting of various types of diagnostic methods is proposed. By activating corresponding diagnostic methods in each part, the proposed strategy can diagnose all types of IGBT OCFs. The main contributions of the proposed switching method and the improved switching method-based diagnostic strategy are summarized as follows.

1) The improved switching method-based diagnostic strategy proposed in this paper addresses the gap in IGBT OCF diagnosis for HMMCs, which can diagnose all types of IGBT OCFs of HMMCs within 20 ms.
2) The improved switching method proposed in this paper eliminates the adverse effects of the existing switching method, which can ensure that all types of IGBT OCFs reveal their fault characteristics thoroughly and keep the switching loss unchanged compared to the existing switching method.
3) The improved switching method-based diagnostic strategy proposed in this paper has a wide range of applications

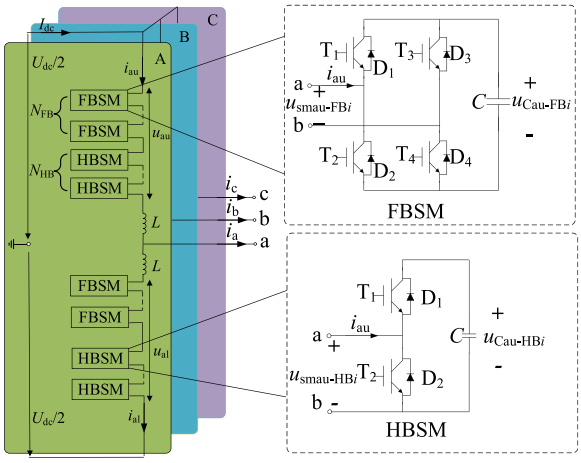

Fig. 1. Topology of an HMMC.

TABLE I
FBSM OPERATING MODES IN NORMAL STATE

Mode	i_{arm}	$S_{Fun-FBi}$	S_{FBi}	Path	SM state	u_{C-FBi}
1	$\geqslant 0$	1	1	D_1, D_4	Positively-insert	↑
2		-1	2	T_2, T_3	Negatively-insert	↓
3		0	3	D_1, T_3	Bypass	—
4		0	4	T_2, D_4	Bypass	—
5	<0	1	1	T_1, T_4	Positively-insert	↓
6		-1	2	D_2, D_3	Negatively-insert	↑
7		0	3	T_1, D_3	Bypass	—
8		0	4	D_2, T_4	Bypass	—

that are also applicable to HBMMCs and FBMMCs and has immunity to dc faults and load change.

The rest of this article is organized as follows: Section II introduces the basic configuration and operating principles of HMMCs. Section III introduces the existing switching method and proposes an improved switching method. The fundamental characteristics of IGBT OCFs are analyzed in Section IV. The advantages of the proposed switching method are also highlighted based on the comparisons of IGBT OCF characteristics under two switching methods in Section IV. The switching sequence characteristics of normal SMs and SMs under IGBT OCFs in the HMMC are analyzed in detail in Section V. The improved switching method-based diagnostic strategy is proposed in Section VI. Further discussions of the proposed improved switching method and the improved switching method-based diagnostic strategy are given in Section VII. The comprehensive hardware-in-the-loop (HIL) experimental results are given in Section VIII. Finally, Section IX concludes this article.

II. Basic Configurations and Operating Principles of HMMCs

A. Basic Configurations of HMMCs

The topology of a three-phase six-arm HMMC is shown in Fig. 1. Each arm includes N SMs and one arm inductor L. Among N SMs, there are N_{FB} FBSMs and N_{HB} HBSMs. The ratio N_{FB}/N is the SM hybrid ratio. U_{dc} and I_{dc} are the dc-side voltage and current, respectively. i_{ju}, i_{jl} represent the upper arm current and the lower arm current, respectively. u_{ju} and u_{jl} represent the output voltages of all the SMs in the upper arm and in the lower arm, respectively. The topologies of the FBSM and the HBSM are also shown in Fig. 1. u_{Ci} and $u_{\mathrm{sm}i}$ represent the capacitor voltage and the output voltage of the SM, respectively. To distinguish between variables related to the FBSM and HBSM, this article uses the "FB" and "HB" in the subscripts, where the variable with "FB" is associated with FBSMs and the variable with "HB" is associated with HBSMs. The "a," "b," and "c" in the subscripts stand for variables related to Phase A, Phase B, and Phase C, respectively. The "u" and "l" in the subscripts stand for variables related to the upper arm and lower arm.

For an FBSM, it has eight modes as shown in Table I, where $S_{\mathrm{FB}i}$ and $S_{\mathrm{Fun\text{-}FB}i}$ represent the switching sequence and the switching function of the FBSM, respectively. i_{arm} represent the arm current. During the normal operation, $S_{\mathrm{Fun\text{-}FB}i}$ is controlled by the voltage balancing strategy (VBS) as follows:

$$S_{\mathrm{Fun\text{-}FB}i}=\begin{cases}1, & \text{when SM needs to be inserted positively}\\ 0, & \text{when SM needs to be bypassed}\\ -1, & \text{when SM needs to be inserted negatively.}\end{cases} \tag{1}$$

In an FBSM, its $u_{\mathrm{sm\text{-}FB}i}$ is controlled by $S_{\mathrm{Fun\text{-}FB}i}$ as follows:

$$u_{\mathrm{sm\text{-}FB}i}=S_{\mathrm{Fun\text{-}FB}i}u_{C\text{-}\mathrm{FB}i}. \tag{2}$$

The value of $S_{\mathrm{FB}i}$ depends on the value of $S_{\mathrm{Fun\text{-}FB}i}$ as follows:

$$S_{\mathrm{FB}i}=\begin{cases}1, & S_{\mathrm{Fun\text{-}FB}i}=1\\ 2, & S_{\mathrm{Fun\text{-}FB}i}=-1\\ 3, & S_{\mathrm{Fun\text{-}FB}i}=0\\ 4, & S_{\mathrm{Fun\text{-}FB}i}=0.\end{cases} \tag{3}$$

Then, switching states of the T_1, T_2, T_3, and T_4 in the FBSM can be confirmed based on $S_{\mathrm{FB}i}$, which can be expressed as

$$S_{\mathrm{FB}i}=\begin{cases}1, & \mathrm{T}_1 \text{ and } \mathrm{T}_4 \text{ are ON while } \mathrm{T}_2 \text{ and } \mathrm{T}_3 \text{ are OFF}\\ 2, & \mathrm{T}_2 \text{ and } \mathrm{T}_3 \text{ are ON while } \mathrm{T}_1 \text{ and } \mathrm{T}_4 \text{ are OFF}\\ 3, & \mathrm{T}_1 \text{ and } \mathrm{T}_3 \text{ are ON while } \mathrm{T}_2 \text{ and } \mathrm{T}_4 \text{ are OFF}\\ 4, & \mathrm{T}_2 \text{ and } \mathrm{T}_4 \text{ are ON while } \mathrm{T}_1 \text{ and } \mathrm{T}_3 \text{ are OFF.}\end{cases} \tag{4}$$

For an HBSM, it has four modes as shown in Table II, where $S_{\mathrm{HB}i}$ and $S_{\mathrm{Fun\text{-}HB}i}$ represent the switching sequence and the switching function of the HBSM. Similar to the FBSM, $S_{\mathrm{Fun\text{-}HB}i}$ is also controlled by the VBS as:

$$S_{\mathrm{Fun-HB}i}=\begin{cases}1, & \text{when SM needs to be inserted positively.}\\ 0, & \text{when SM needs to be bypassed.}\end{cases} \tag{5}$$

In an HBSM, its $u_{\mathrm{sm\text{-}HB}i}$ is controlled by $S_{\mathrm{Fun\text{-}HB}i}$ as follows:

$$u_{\mathrm{sm-HB}i}=S_{\mathrm{Fun-HB}i}u_{C-\mathrm{HB}i}. \tag{6}$$

TABLE II
HBSM OPERATING MODES IN NORMAL STATE

Mode	i_{arm}	$S_{Fun\text{-}HBi}$	S_{HBi}	Path	SM state	$u_{C\text{-}HBi}$
1	$\geqslant 0$	1	1	D_1	Positively-insert	↑
2		0	2	T_2	Bypass	—
3	<0	1	1	T_1	Positively-insert	↓
4		0	2	D_2	Bypass	—

The value of $S_{\mathrm{HB}i}$ depends on the value of $S_{\mathrm{Fun\text{-}HB}i}$ as follows:

$$S_{\mathrm{HB}i} = \begin{cases} 1, & S_{\mathrm{Fun-HB}i} = 1 \\ 2, & S_{\mathrm{Fun-HB}i} = 0. \end{cases} \tag{7}$$

Then, switching states of the T_1, T_2 in the HBSM can be confirmed based on $S_{\mathrm{HB}i}$, which can be expressed as follows:

$$S_{\mathrm{HB}i} = \begin{cases} 1, & \mathrm{T}_1 \text{ is ON while } \mathrm{T}_2 \text{ is OFF} \\ 2, & \mathrm{T}_2 \text{ is ON while } \mathrm{T}_1 \text{ is OFF.} \end{cases} \tag{8}$$

B. Operating Principles of HMMCs

Defining M_{ac} as the ac modulation index of the HMMC, which can be expressed as follows:

$$M_{\mathrm{ac}} = \frac{U_{\mathrm{m}}}{0.5U_{\mathrm{dcn}}} \tag{9}$$

where U_{m} and U_{dcn} represent the amplitude of the output ac voltage and the rated dc voltage, respectively.

According to papers [4], [5], and [10], the HMMC can still output rated ac voltage under low dc voltages, thus a dc modulation index M_{dc} can be defined as follows:

$$M_{\mathrm{dc}} = \frac{U_{\mathrm{dc}}}{U_{\mathrm{dcn}}}. \tag{10}$$

According to paper [4], the range of u_{au} and u_{al} can be obtained as follows:

$$0.5U_{\mathrm{dcn}}(M_{\mathrm{dc}} - M_{\mathrm{ac}}) \leq \{u_{\mathrm{au}}, u_{\mathrm{al}}\} \leq 0.5U_{\mathrm{dcn}}(M_{\mathrm{dc}} + M_{\mathrm{ac}}). \tag{11}$$

It can be observed from (11) that the u_{au} and u_{al} have the same range. Thus, this article only targets at u_{au} for analysis. Based on the analysis in Section II-A, u_{au} is the output voltages of all the SMs in the upper arm, which can be expressed as follows:

$$u_{\mathrm{au}} = \sum_{i=1}^{i=N_{\mathrm{FB}}} S_{\mathrm{Funau\text{-}FB}i} u_{C\mathrm{au\text{-}FB}i} + \sum_{i=1}^{i=N_{\mathrm{HB}}} S_{\mathrm{Funau-HB}i} u_{C\mathrm{au-HB}i}. \tag{12}$$

When the HMMC is not operating under overmodulation or low dc voltage scenario, there exists $M_{\mathrm{ac}} < 1$ and $M_{\mathrm{dc}} = 1$. Under this operating condition, it can be obtained from (11) that u_{au} is always positive, which means the arm need not generate negative voltage. Thus, the negatively inserted state of FBSMs is not used and the HMMC operates in the same way as the HBMMC do [10]. When $M_{\mathrm{ac}} > 1$ or $M_{\mathrm{dc}} < 1$, it can be obtained from (11) that u_{au} needs to be a negative value, which means the arm needs to generate negative voltage. According to (12), some FBSMs need to work in the negatively-inserted state to generate negative voltage, whose switching functions are -1. Based on the negatively inserted state of FBSM, the HMMC can output rated ac voltage under low dc voltage or output high ac voltage under rated dc voltage, which cannot be realized in the HBMMC.

C. Generating Process of the Driving Signals to IGBTs

The flowchart of the VBS adopted in the HMMC is depicted in Fig. 2 [10], where N_{on} and $N_{\mathrm{on\text{-}pre}}$ represent the number of inserted SMs in the current control period and previous control period, respectively. When $N_{\mathrm{on}} \geq 0$, the VBS does not discriminate between FBSMs and HBSMs and the VBS is the same as the VBS adopted in the HBMMC. When $N_{\mathrm{on}} < 0$, only FBSMs are used while all HBSMs are bypassed.

The generating process of the driving signals to IGBTs is shown in Fig. 3, where $N_{\mathrm{on}\text{-}jx}$ is the number of inserted SMs in the x arm of phase j. The function of the switching method is to output proper switching sequences based on switching functions, whose working process will be introduced in detail in the next section. Finally, the driving signal generator generates proper driving signals based on switching sequences according to (4) and (8).

III. PROPOSED IMPROVED SWITCHING METHOD OF FBSMs

The switching method of HBSMs is unique because the $S_{\mathrm{HB}i}$ and $S_{\mathrm{Fun\text{-}HB}i}$ are on a one-to-one correspondence basis according to (7). Therefore, this section focuses on the switching method of FBSMs.

The flowchart of the existing switching method is shown in Fig. 4 [25]. When $S_{\mathrm{Fun\text{-}FB}i}$ equals $S_{\mathrm{Fun\text{-}FB}i\text{-}\mathrm{pre}}$, it indicates that the switching function does not need to change at the current period. Thus, the switching sequence remains unchanged at the current period. When $S_{\mathrm{Fun\text{-}FB}i}$ does not equal $S_{\mathrm{Fun\text{-}FB}i\text{-}\mathrm{pre}}$, it indicates the switching function needs to change at the current period. Then, the switching sequence can be derived based on the following equation:

$$S_{\mathrm{FB}i} = \begin{cases} 1, & S_{\mathrm{Fun\text{-}FB}i} = 1 \\ 2, & S_{\mathrm{Fun\text{-}FB}i} = -1 \\ 4, & S_{\mathrm{Fun\text{-}FB}i} = 0. \end{cases} \tag{13}$$

The flowchart of the improved switching method proposed in this article is shown in Fig. 5, where $F_{\mathrm{FB}i}$ represents the flag for the bypassed switching sequence selection. $F_{\mathrm{FB}i}$ is a logical signal that can be 1 or 0, corresponding to the two bypassed switching sequences of the FBSM. $F_{\mathrm{FB}i}$ can be determined based on the following equation:

$$F_{\mathrm{FB}i} = \begin{cases} !F_{\mathrm{FB}i}, & S_{\mathrm{Fun\text{-}FB}i} \neq S_{\mathrm{Fun\text{-}FB}i-\mathrm{pre}} \text{ and } S_{\mathrm{Fun\text{-}FB}i} = 1 \\ F_{\mathrm{FB}i}, & \text{in other cases.} \end{cases} \tag{14}$$

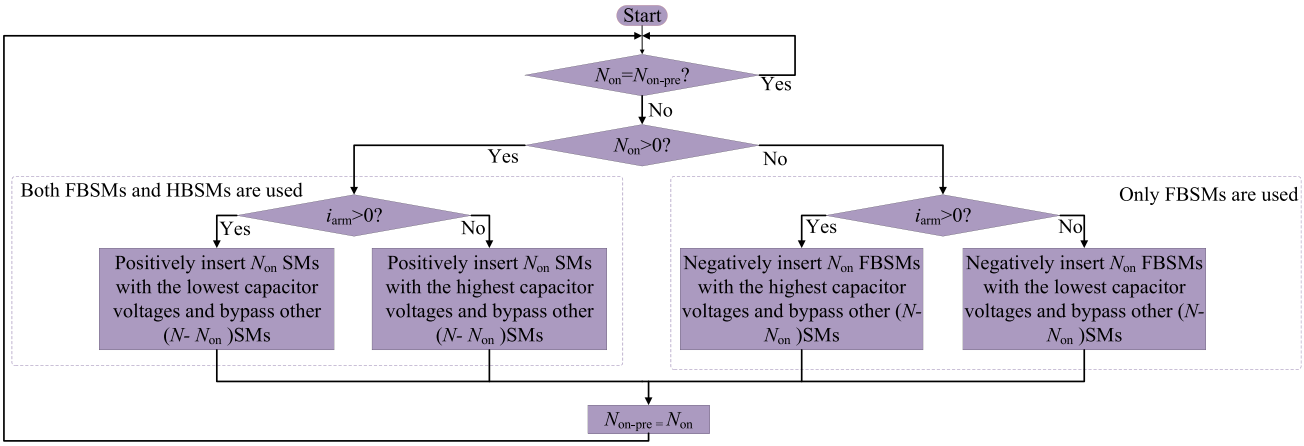

Fig. 2. VBS in the HMMCs.

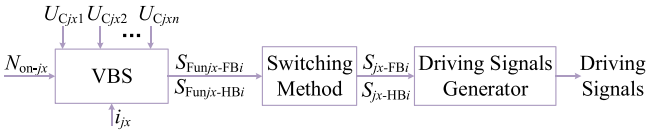

Fig. 3. Generation process of the driving signals.

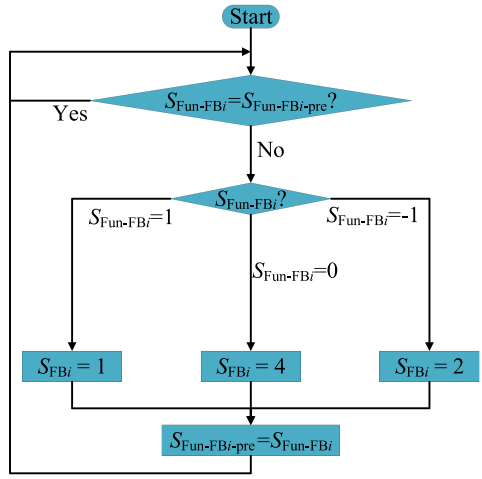

Fig. 4. Flowchart of the existing switching method.

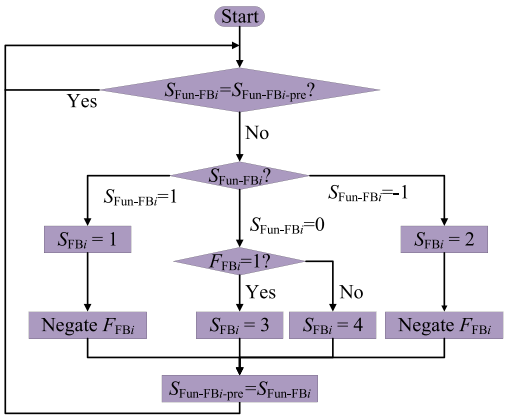

Fig. 5. Flowchart of the proposed improved switching method.

According to (14), when $S_{\text{Fun-FB}i}$ does not equal $S_{\text{Fun-FB}i\text{-pre}}$ and $S_{\text{Fun-FB}i}$ is 1, $F_{\text{FB}i}$ needs to be inverted. While in other cases, $F_{\text{FB}i}$ remains unchanged.

When $S_{\text{Fun-FB}i}$ equals $S_{\text{Fun-FB}i\text{-pre}}$, the switching sequence also remains unchanged at the current period. When $S_{\text{Fun-FBi}}$ does not equal $S_{\text{Fun-FB}i\text{-pre}}$, the switching sequence can be derived based on the following equation:

$$S_{\text{FB}i} = \begin{cases} 1, & S_{\text{Fun-FB}i} = 1 \\ 2, & S_{\text{Fun-FB}i} = -1 \\ 3, & S_{\text{Fun-FB}i} = 0 \text{ and } F_{\text{FB}i} = 1 \\ 4, & S_{\text{Fun-FB}i} = 0 \text{ and } F_{\text{FB}i} = 0. \end{cases} \tag{15}$$

By introducing the bypassed switching sequence selection flag, the corresponding switching sequence alternates between the two bypassed switching sequences when the FBSM transitions from the positively inserted state or the negatively inserted state to the bypassed state. In contrast to the existing switching method, the switching sequence can take 1, 2, 3, and 4 under the proposed switching method, while the switching sequence can only take 1, 2, and 4 under the existing switching method. Based on Table I, it can be observed that the proposed switching method contains all eight modes of the FBSM, while the existing switching method misses Mode 3 and Mode 7.

Due to the complement of the missing Mode 3 and Mode 7, IGBT OCFs can more fully reflect their fault characteristics under the proposed switching method compared to the existing switching method, which will be analyzed in detail in Section IV-C.

IV. Fundamental Characteristics of IGBT OCFs

A. Characteristics of IGBT OCFs in HBSMs

The IGBT OCFs of an HBSM can be categorized into two types: Type I_{HB} fault and Type II_{HB} fault, corresponding to T_1 and T_2 OCF, respectively. These two types of faults can disrupt the normal operation of the HBSM, as summarized in Table III. Type I_{HB} fault affects the operation in Mode 3, where the capacitor is bypassed instead of being discharged as shown in

TABLE III
ABNORMAL MODES IN IGBT OPEN-CIRCUIT FAULTS

Type	Abnormal OP	Path	SM state	u_{Ci}
Type I_{HB}	3	$T_1 \rightarrow D_2$	Bypass	—
Type II_{HB}	2	$T_2 \rightarrow D_1$	Positively-insert	↑
Type I_{FB}	5	$T_1, T_4 \rightarrow T_4, D_2$	Bypass	—
	7	$T_1, D_3 \rightarrow D_2, D_3$	Negatively-insert	↑
Type II_{FB}	2	$T_2, T_3 \rightarrow D_1, T_3$	Bypass	—
	4	$T_2, D_4 \rightarrow D_1, D_4$	Positively-insert	↑
Type III_{FB}	2	$T_2, T_3 \rightarrow T_2, D_4$	Bypass	—
	3	$D_1, T_3 \rightarrow D_1, D_4$	Positively-insert	↑
Type IV_{FB}	5	$T_1, T_4 \rightarrow D_3, T_1$	Bypass	—
	8	$D_2, T_4 \rightarrow D_2, D_3$	Negatively-insert	↑

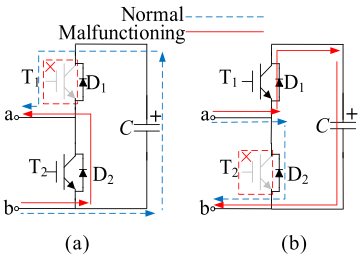

Fig. 6. Two abnormal modes of IGBT OCFs in HBSMs. (a) Mode 3 of type I_{HB} fault. (b) Mode 2 of type II_{HB} fault.

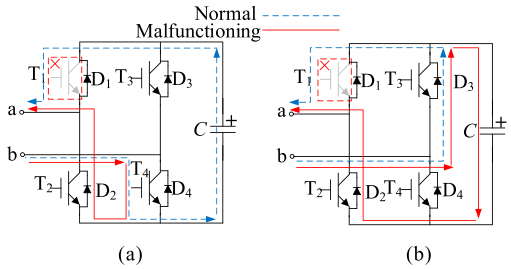

Fig. 7. Two abnormal modes of Type I_{FB} fault. (a) Mode 5. (b) Mode 7.

Fig. 6(a). Type II_{HB} fault affects the operation in Mode 2, where the capacitor is charged instead of being bypassed as shown in Fig. 6(b).

B. Characteristics of IGBT OCFs in FBSMs

An FBSM has more complex IGBT OCFs than those of an HBSM, as it can be classified into four types. These four types are Type I_{FB} fault, Type II_{FB} fault, Type III_{FB} fault and Type IV_{FB} fault, corresponding to T_1, T_2, T_3, and T_4 OCF, respectively. Table III summarizes how these four types of faults can affect the normal operations of an FBSM. As depicted in Fig. 7, Type I_{FB} fault affects the operations in Mode 5 and Mode 7, where the capacitor is bypassed instead of being discharged in Mode 5 and the capacitor is charged instead of being bypassed in Mode 7. Similarly, the affected operations of Type II_{FB} fault, Type III_{FB} fault, and Type IV_{FB} fault are shown in Figs. 8–10, respectively.

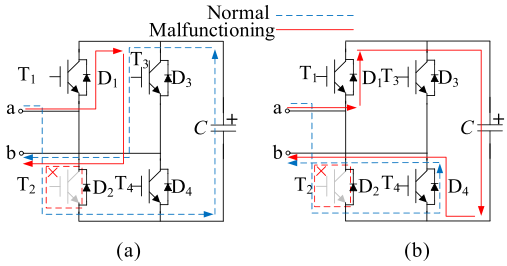

Fig. 8. Two abnormal modes of Type II_{FB} fault. (a) Mode 2. (b) Mode 4.

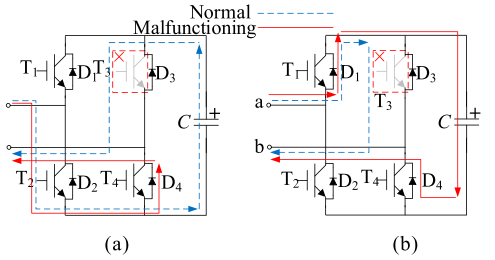

Fig. 9. Two abnormal modes of type III_{FB} fault. (a) Mode 2. (b) Mode 3.

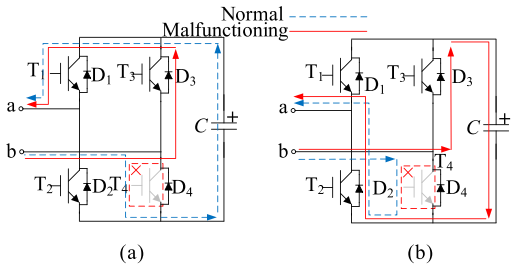

Fig. 10. Two abnormal modes of type IV_{FB} fault. (a) Mode 5. (b) Mode 8.

C. Comparisons of IGBT OCF Fault Characteristics in FBSMs Under Two Switching Methods

The four parts can be divided according to the polarity of the arm current and the polarity of the number of inserted SMs. In Part I, both the arm current and the number of inserted SMs are positive. In Part II, the arm current is positive and the number of inserted SMs is negative. In Part III, both the arm current and the number of inserted SMs are negative. In Part IV, the arm current is negative and the number of inserted SMs is positive. According to paper [27], the existence of Part II and Part III depends on the operating mode of the HMMC. For example, the numbers of inserted SMs and arm current under two operating modes are shown in Fig. 11. It can be observed from Fig. 11(a) that only Part I, Part III, and Part IV exist when the HMMC operates in the rectifier mode. Regarding the inverter mode, it can be seen from Fig. 11(b) that only Part I, Part II, and Part IV exist.

Combing Fig. 4 and Table III, the abnormal modes of IGBT OCFs in FBSMs and their corresponding parts under the existing switching method can be depicted in Fig. 12. A comparison of Table III and Fig. 12 reveals that certain fault characteristics of

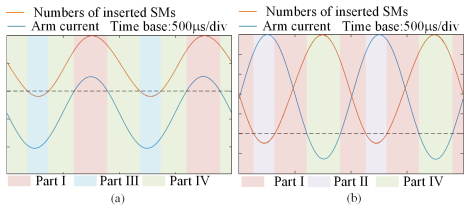

Fig. 11. Arm current and number of inserted SMs in HMMCs under two operating modes. (a) Rectifier mode. (b) Inverter mode.

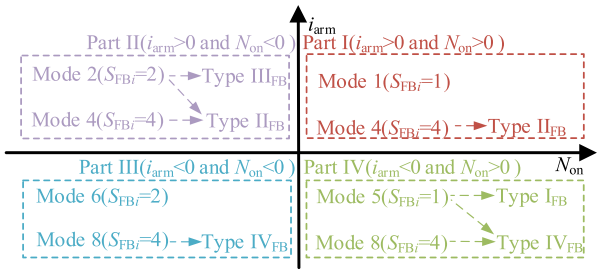

Fig. 12. Abnormal modes of IGBT OCFs in FBSMs under the existing switching method.

the Type I_{FB} fault and the Type III_{FB} fault are missing due to the absence of Mode 3 and Mode 7, which are not beneficial to their diagnosis. The Type I_{FB} fault cannot exhibit fault characteristics in Part III. When the HMMC operates in rectifier mode and a Type I_{FB} fault occurs in Part III, the Type I_{FB} fault cannot be diagnosed in Part III and can only be diagnosed in the next Part IV, which prolongs the time required for diagnosis. The Type III_{FB} fault is more severely affected and it can only exhibit fault characteristics in Mode 2 of Part II. However, when the HMMC operates in rectifier mode, only Part I, Part III, and Part IV exist, which results in a complete miss of fault characteristics for Type III_{FB} fault, and thus cannot be diagnosed. When the HMMC operates in inverter mode, although Part II exists, the number of negatively-inserted SMs is low due to the presence of dc voltage bias [4], [10]. Therefore, the probability of a Type III faulty SM being able to operate in Mode 2 is lower, which may prolong the time required for diagnosis and is likewise detrimental to its diagnosis.

Based on the above analysis, the absence of Mode 3 and Mode 7 in the existing switching method is not conducive to the diagnosis of some types of IGBT OCFs and may result in specific IGBT OCFs not being diagnosed. Therefore, this article proposes an improved switching method that complements the missing Mode 3 and Mode 7. Combing Fig. 5 and Table III, the abnormal modes of IGBT OCFs in FBSMs and their corresponding parts under the improved switching method can be depicted in Fig. 13. A comparison of Figs. 12 and 13 reveals that the improved switching method can completely reflect the fault characteristics of the Type I_{FB} fault, which is advantageous for its fault diagnosis. More importantly, Type III_{FB} faults can not only reflect the fault characteristics in Part II but also in Part I, which is common to both rectifier mode and inverter mode. This avoids the problems of undiagnostic in rectifier mode and potentially long diagnostic time in inverter mode.

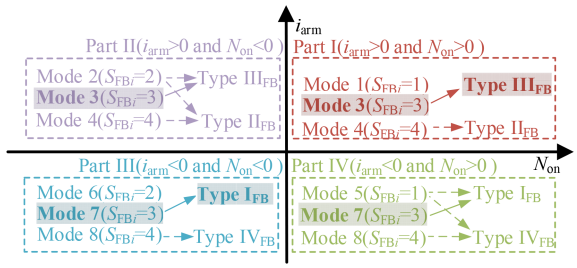

Fig. 13. Abnormal modes of IGBT OCFs in FBSMs under the proposed improved switching method.

Based on the above analysis, compared to the existing switching method, the proposed improved switching method enables IGBT OCFs in FBSMs to reflect their fault characteristics more thoroughly, which is beneficial for the subsequent diagnosis of IGBT OCFs.

V. Switching Sequence Characteristic of Normal SMs and SMs Under IGBT OCFs in the HMMC

A. Switching Sequence Characteristic of Normal SMs in the HMMC

The objective of the VBS is to maintain the dynamic balance of the SM capacitor voltages within the arm. To achieve this objective, the switching functions of normal SMs are in the dynamic change in most cases to adjust the charging and discharging time of capacitors. Correspondingly, the switching sequences of normal SMs are in the state of dynamic change in most cases [11], [28]. For the HMMC, its switching sequence characteristic are a little bit more complicated. In Part II and Part III, only FBSMs are used. Therefore, the switching sequences of normal FBSMs are in a dynamic change in these two parts. In Part I and Part IV, the switching sequences of normal FBSMs and HBSMs are all in dynamic change when the SM capacitor voltages of two types are basically the same. However, there may exist a special period in which the switching sequences of normal SMs remain at a specific value. For example, when the HMMC operates in inverter mode, FBSMs are being negatively-inserted in turns and all HBSMs are bypassed in Part II. Therefore, a capacitor voltage deviation between FBSMs and HBSMs is generated since the capacitor voltages of FBSMs grow lower and the capacitor voltages of HBSMs remain unchanged. Then, even though the VBS does not discriminate FBSMs from HBSMs in the adjacent Part I, the inserted prioritization of the FBSMs is higher than HBSMs in the next Part I until the capacitor voltages of the two types of SMs are basically the same. Before that, the switching sequences of normal FBSMs are still in the dynamic change, while the switching sequences of normal HBSMs are not dynamic but remain at 2.

Based on the analysis, the switching sequences of normal SMs with the same type in the HMMC always have consistent trends. In particular, the switching sequences of normal SMs with the same type are all in the state of dynamic change in most cases or all remaining at a specific value in special cases. However, the switching sequence of the faulty SM has a different

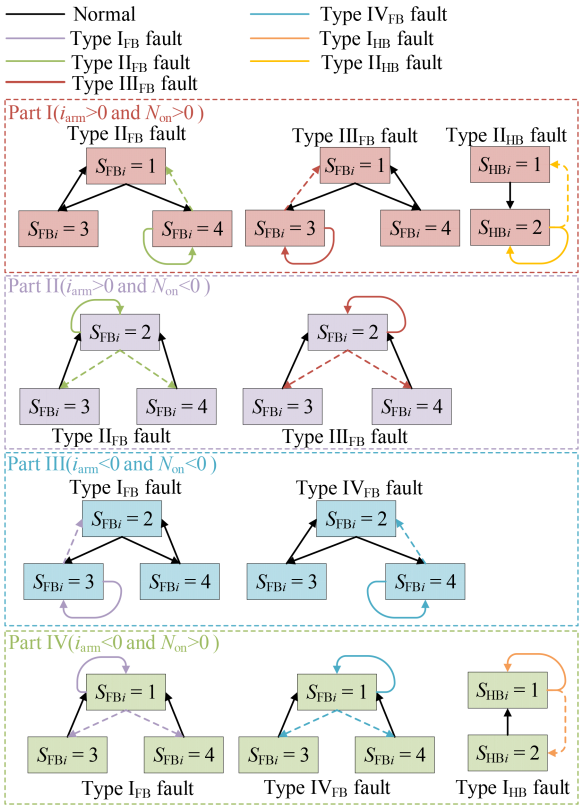

Fig. 14. Switching process for different types of IGBT OCFs.

trend from the normal SM, which will be analyzed in detail as follows.

B. Switching Sequence Characteristic of SMs Under IGBT OCFs in the HMMC

Based on the analysis in Section IV-C, four types of IGBT OCFs in FBSM can exhibit their fault characteristics thoroughly under the proposed improved switching method. As for two types of IGBT OCFs in HBSM, the Type $\mathrm{I_{HB}}$ fault can exhibit its fault characteristic in Part IV, Type $\mathrm{II_{HB}}$ fault can exhibit its fault characteristic in Part I and Part II based on Table III. On this basis, the switching sequence characteristics of IGBT OCFs under the proposed switching method are analyzed in this section. The switching sequence of the faulty SM remains at a specific value during a specific part. The detailed characteristics are analyzed as follows.

1) Part I: Based on Fig. 13 and the above analysis, Type $\mathrm{II_{FB}}$ malfunctioning SM, Type $\mathrm{III_{FB}}$ malfunctioning SM, and Type $\mathrm{II_{HB}}$ malfunctioning SM exhibit fault characteristics in Part I.

For a Type $\mathrm{II_{FB}}$ malfunctioning SM, it operates normally in all modes except for Mode 4, where its $S_{\mathrm{FB}i}$ is 4. As shown in Fig. 14, if the $S_{\mathrm{FB}i}$ of the malfunctioning SM does not switch to 4, its $S_{\mathrm{FB}i}$ still switches like a normal FBSM. Once the $S_{\mathrm{FB}i}$ of the malfunctioning SM switches to 4 under the control of VBS and the proposed switching method, it indicates that its capacitor voltage is relatively higher in the arm and should remain unchanged. However, the capacitor of the malfunctioning SM is charged instead of being bypassed in Mode 4, causing the rise of its voltage. Therefore, a conflict between the control objective of the VBS and the impact of the Type $\mathrm{II_{FB}}$ fault creates. Correspondingly, the VBS forces the malfunctioning SM to remain bypassed to prevent its capacitor voltage from increasing, which exacerbates the conflict continuously. Finally, the improved switching method forces the $S_{\mathrm{FB}i}$ of malfunctioning SM to be 4 as shown in Part I of Fig. 14. For a Type $\mathrm{III_{FB}}$ fault, its analysis process is similar to that of the Type $\mathrm{II_{FB}}$ fault. The improved switching method forces the $S_{\mathrm{FB}i}$ of the malfunctioning SM to be 3 in Part I as shown in Fig. 14.

For a Type $\mathrm{II_{HB}}$ malfunctioning SM, it operates normally except for Mode 2. Once the $S_{\mathrm{HB}i}$ of malfunctioning SM switches to 2 under the control of VBS and the switching method, it indicates that its capacitor voltage is relatively higher in the arm and should remain unchanged. However, the capacitor of the malfunctioning SM is charged instead of being bypassed in Mode 2, causing the rise of its voltage. Therefore, a conflict between the control objective of the VBS and the impact of the Type $\mathrm{II_{HB}}$ fault creates. Correspondingly, the VBS forces the malfunctioning SM to remain bypassed to prevent its capacitor voltage from increasing, which exacerbates the conflict continuously. Finally, the switching method forces the $S_{\mathrm{HB}i}$ of malfunctioning SM to be 2 as shown in Part I of Fig. 14.

2) Part II: Based on Fig. 13 and the above analysis, Type $\mathrm{II_{FB}}$ malfunctioning SM, Type $\mathrm{III_{FB}}$ malfunctioning SM and Type $\mathrm{II_{HB}}$ malfunctioning SM exhibit fault characteristics in Part II.

For a Type $\mathrm{II_{FB}}$ malfunctioning SM, it operates normally except for Mode 2 and Mode 4, where its $S_{\mathrm{FB}i}$ is 2 and 4, respectively. If the $S_{\mathrm{FB}i}$ of the malfunctioning SM switches to 4 under the control of VBS and the proposed switching method, it indicates that the capacitor voltage of the malfunctioning SM is relatively lower in the arm and should remain unchanged. Due to the fault behavior in Mode 4, the capacitor of the malfunctioning SM is charged instead of being bypassed, causing the rise of its voltage. Therefore, the VBS controls the malfunctioning SM to switch from the bypassed state to the negatively inserted state after a period of time. Once the $S_{\mathrm{FB}i}$ of the malfunctioning SM switches to 2 under the control of VBS and the proposed switching method, it indicates that its capacitor voltage is relatively higher in the arm and should grow low. However, the capacitor of the malfunctioning SM is bypassed instead of being discharged in Mode 2, causing its voltage to remain unchanged. Therefore, a conflict between the control objective of the VBS and the impact of the Type $\mathrm{II_{HB}}$ fault creates. Correspondingly, the VBS forces the malfunctioning SM to stay in the negatively-inserted state to make its capacitor voltage grow higher, which exacerbates the conflict continuously. Finally, the improved switching method forces the $S_{\mathrm{HB}i}$ of malfunctioning SM to be 2 as shown in Part II of Fig. 14. For a Type $\mathrm{III_{FB}}$ fault, its analysis process is similar to that of the Type $\mathrm{II_{FB}}$ fault. The improved switching method forces the $S_{\mathrm{FB}i}$ of the malfunctioning SM to be 2 in Part II as shown in Part II of Fig. 14.

For a Type $\mathrm{II_{HB}}$ malfunctioning SM, it operates normally except for Mode 2, where its $S_{\mathrm{FB}i}$ is 2. In Part II, the VBS controls all HBSMs to operate in the bypassed state, while the switching

method controls the $S_{\mathrm{HB}i}$s to be 2 accordingly. Since all the $S_{\mathrm{HB}i}$s remain consistent in this part, the switching sequence characteristic of the Type $\mathrm{II}_{\mathrm{HB}}$ malfunctioning SM is hidden.

3) Part III: Based on Fig. 13 and the above analysis, Type I_{FB} malfunctioning SM and Type $\mathrm{IV}_{\mathrm{FB}}$ malfunctioning SM exhibit fault characteristics in Part III.

For a Type I_{FB} malfunctioning SM, it operates normally in all modes except Mode 7, where its $S_{\mathrm{FB}i}$ is 3. The analysis process of the Type $\mathrm{III}_{\mathrm{FB}}$ fault in Part III is similar to that of the Type $\mathrm{II}_{\mathrm{FB}}$ fault in Part I. The proposed switching method forces the $S_{\mathrm{FB}i}$ of the malfunctioning SM to be 3 as shown in Part III of Fig. 14. For a Type $\mathrm{IV}_{\mathrm{FB}}$ malfunctioning SM, its analysis process of the Type $\mathrm{IV}_{\mathrm{FB}}$ fault in Part III is also similar to that of the Type $\mathrm{II}_{\mathrm{FB}}$ fault in Part I. The proposed switching method forces the $S_{\mathrm{FB}i}$ of the malfunctioning SM to be 4 as shown in Part III of Fig. 14.

4) Part IV: Based on Fig. 13 and the above analysis, Type I_{FB} malfunctioning SM, Type $\mathrm{IV}_{\mathrm{FB}}$ malfunctioning SM, and Type I_{HB} malfunctioning SM exhibit fault characteristics in Part IV.

For a Type I_{FB} malfunctioning SM, it operates normally in all modes except Mode 5 and Mode 7, where its $S_{\mathrm{FB}i}$ is 1 and 3, respectively. The analysis process of the Type I_{FB} fault in Part IV is similar to that of the Type $\mathrm{II}_{\mathrm{FB}}$ fault in Part II. The improved switching method forces the $S_{\mathrm{FB}i}$ of the malfunctioning SM to be 1 as shown in Part IV of Fig. 14. For a Type $\mathrm{IV}_{\mathrm{FB}}$ malfunctioning SM, its analysis process of the Type $\mathrm{IV}_{\mathrm{FB}}$ fault in Part IV is similar to that of the Type $\mathrm{II}_{\mathrm{FB}}$ fault in Part II. The proposed switching method forces the $S_{\mathrm{FB}i}$ of the malfunctioning SM to be 1 in Part III of Fig. 14.

For a Type I_{HB} malfunctioning SM, it operates normally except for Mode 3. Once the $S_{\mathrm{HB}i}$ of the malfunctioning SM switches to 1 under the control of VBS and switching method, it indicates that its capacitor voltage is relatively higher and should decrease. However, the capacitor of the malfunctioning SM is bypassed instead of being discharged in Mode 3, causing its voltage to remain unchanged. Therefore, a conflict between the control objective of the VBS and the impact of the Type $\mathrm{II}_{\mathrm{FB}}$ fault creates. Correspondingly, the VBS forces the malfunctioning SM to remain in the positively inserted state as much as possible to make its capacitor voltage grow lower, which exacerbates the conflict continuously. Finally, the switching method forces the $S_{\mathrm{FB}i}$ of the malfunctioning SM to be 1 in Part IV as shown in Fig. 14.

Based on the above analysis, the switching sequence is a significant fault characteristic for IGBT OCFs in HMMCs. This finding provides a theoretical basis for the improved switching method-based diagnostic strategy proposed in the next section.

VI. Proposed Improved Switching Method-Based Fault Diagnostic Strategy

A. Proposed Improved Switching Method-based Fault Diagnostic Strategy

Based on the analysis in Section V, all six types of malfunctioning SMs remain in specific switching sequences in the corresponding parts while the switching sequences of normal SMs with the same type in the HMMC are all in dynamic change in most cases or all remain at a specific value in special cases.

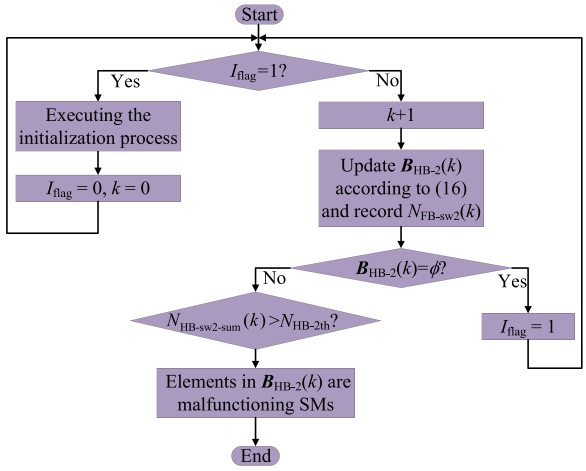

Fig. 15. Diagnostic process for identifying the type $\mathrm{II}_{\mathrm{HB}}$ malfunctioning SM in Part I.

To avoid mistaking the normal SM as the faulty SM, an SM is diagnosed as a faulty SM only if the SM remains in a specific sequence for a period of time while the switching sequences of other SMs with the same type are still dynamically changing. Therefore, a diagnostic method is proposed to identify the SM with the fixed specific sequence in a period of time while the switching sequences of other SMs with the same type are still dynamic. Taking the diagnostic method of identifying the Type $\mathrm{II}_{\mathrm{HB}}$ malfunctioning SM in Part I as an example to illustrate how the proposed method works, whose flowchart is shown in Fig. 15. $B_{\mathrm{HB\text{-}2}}$ represents the set of HBSMs whose switching sequence remains in 2. $A_{\mathrm{HB\text{-}2}}$ represents the set of HBSMs whose switching sequence equals to 2. $N_{\mathrm{HB\text{-}2}}$ is the number of elements in $A_{\mathrm{HB\text{-}2}}$. $N_{\mathrm{HB\text{-}2th}}$ is the diagnostic threshold. $N_{\mathrm{HB\text{-}sw2}}$ is the number of HBSMs whose switching sequence switches from 2 to 1 at a control period. $N_{\mathrm{HB\text{-}sw2\text{-}sum}}$ is the sum of the $N_{\mathrm{HB\text{-}sw2}}$ during several control periods. I_{flag}, k are the initial flag and the counting flag, respectively. The initial value of I_{flag} is 0. Therefore, the initialization process is executed firstly as shown in Fig. 15. $B_{\mathrm{HB\text{-}2}}(0)$ is initialized as the $A_{\mathrm{HB\text{-}2}}(0)$. Then, $N_{\mathrm{HB\text{-}2th}}$ is selected based on $N_{\mathrm{HB\text{-}2}}$, which will be discussed in next section. The initialization process is not executed again unless $B_{\mathrm{HB\text{-}2}}$ becomes an empty set. If I_{flag} does not equal 1, $B_{\mathrm{HB\text{-}2}}(k)$ is updated according to the following:

$$B_{\mathrm{HB-2}}(k) = A_{\mathrm{HB-2}}(k) \cap B_{\mathrm{HB-2}}(k-1). \tag{16}$$

$N_{\mathrm{HB\text{-}sw2}}(k)$ is recorded. $N_{\mathrm{HB\text{-}sw2}}(k)$ can be calculated according to the following equation:

$$N_{\mathrm{HB-sw2-sum}}(k) = \sum_{i=1}^{k} N_{\mathrm{HB-sw2}}(i). \tag{17}$$

To identify the Type $\mathrm{II}_{\mathrm{HB}}$ malfunctioning SM in Part I, two conditions must be met concurrently. The first condition is that the switching sequence of the faulty SM remains in 2 for a period of time. The second condition is that the switching sequence of other HBSMs is dynamically changing during the period of time. To ensure that both conditions are met, it is only necessary

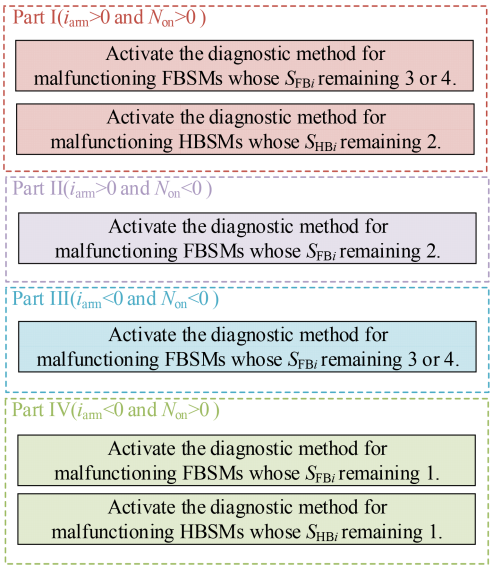

Fig. 16. Overall structure of the proposed diagnostic strategy.

to ensure that $B_{\text{HB-2}}(k)$ is a nonempty set and $N_{\text{HB-sw2-sum}}(k)$ exceeds the diagnostic threshold. $B_{\text{HB-2}}(k)$ is a nonempty set, indicating that there exists HBSMs whose switching sequence remains in 2. The increase in $N_{\text{HB-sw2-sum}}(k)$ reflects the dynamics of switching sequences in normal HBSMs. In particular, if the switching sequences of HBSMs all remain in a specific value as in the aforementioned special case, $N_{\text{HB-sw2}}(k)$ is 0 and $N_{\text{HB-sw2-sum}}(k)$ remains unchanged. Therefore, $N_{\text{HB-sw2-sum}}(k)$ does not exceed $N_{\text{HB-2th}}$ and the diagnostic method does not mistake the normal SM as the faulty SM.

Based on the above analysis, the Type II_{HB} malfunctioning SM can be effectively diagnosed when $B_{\text{HB-2}}(k)$ is a nonempty set and $N_{\text{HB-sw2-sum}}(k)$ exceeds the diagnostic threshold.

The above process targets malfunctioning HBSMs whose $S_{\text{HB}i}$ remains in 2 in Part I, which can be easily adjusted to use for other types of malfunctioning SMs. While adjusting the process, the principle remains unchanged and the parameters change correspondingly. For instance, the method in Fig. 15 can be modified to another method to target malfunctioning FBSMs whose $S_{\text{FB}i}$s remain in 2 in Part II by following adjustments: adjusting $B_{\text{HB-2}}(k)$ to $B_{\text{FB-2}}(k)$, $N_{\text{HB-2th}}$ to $N_{\text{FB-2th}}$, $N_{\text{HB-2}}$ to $N_{\text{FB-2}}$, $N_{\text{HB-sw2}}(k)$ to $N_{\text{FB-sw2}}(k)$, where $B_{\text{FB-2}}(k)$ is the set of potential Type II_{FB} and Type III_{FB} malfunctioning SMs, $N_{\text{FB-2th}}$ is the diagnostic threshold, $N_{\text{FB-2}}$ is the amount of the number of elements in $A_{\text{HB-2}}$, and $N_{\text{FB-sw2}}(k)$ is the number of FBSMs whose switching sequence is transferred from 2 to 3 or 4 from (k-1)T_{c} to kT_{c}. Based on the above method and Fig. 14, a diagnostic strategy for IGBT OCFs in HMMCs can be proposed as shown in Fig. 16. By activating the corresponding methods in each part, the proposed improved switching method-based diagnostic strategy can diagnose all six types of IGBT OCFs. Moreover, it can be observed that the targets of Parts I and IV encompass all six types of faults, the whole diagnosis can be completed within 20 ms regardless of fault type.

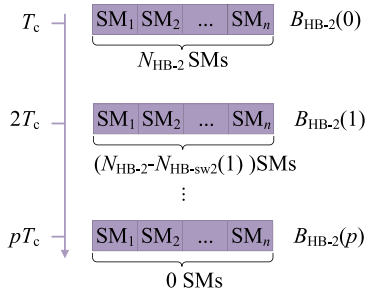

Fig. 17. Executions of the diagnostic process while no type II_{HB} fault existing.

B. Principle of Selection to Diagnostic Threshold

The selection to diagnostic threshold is crucial to the proposed diagnostic strategy, whose principle is discussed in detail in this section.

Taking the $N_{\text{HB-2th}}$ as an example to illustrate the principle of selection to the diagnostic threshold. If there are no Type II_{HB} faults in Part I, the executions of the corresponding diagnostic method can be depicted in Fig. 17. Since the switching sequences of normal HBSMs exhibit dynamic switching processes in most cases, $B_{\text{HB-2}}$ becomes an empty set after a period of time. At time T_{c}, $B_{\text{HB-2}}(0)$ is initialized to $A_{\text{HB-2}}(0)$ and have $N_{\text{HB-2}}$ elements. Assuming it takes p control periods for $B_{\text{HB-2}}$ to become an empty set. Defining $C_{\text{HB-2}}(k)$ is the set that includes $N_{\text{HB-sw2}}(k)$ HBSMs whose $S_{\text{HB}i}$s switch from 2 to 1 in kT_{c}. During each of these p control periods, $C_{\text{HB-2}}(k)$ can be divided into two subsets: the first subset belongs to $B_{\text{HB-2}}(k-1)$ and the second subset does not belong to $B_{\text{HB-2}}(k-1)$. Extremely, if the second subset is always empty in these p control periods, $N_{\text{HB-sw2-sum}}(p)$ can be minimized to $N_{\text{HB-2}}$. In such an extreme case, $N_{\text{HB-2th}}$ only needs to be selected greater than $N_{\text{HB-2}}$. However, $N_{\text{HB-sw2-sum}}(p)$ always takes a higher value than $N_{\text{HB\_2}}$ due to the existence of the second subset. Compared to the elements not in $B_{\text{HB-2}}(k-1)$, the capacitor voltages of elements in $B_{\text{HB-2}}(k-1)$ have remained unchanged for a longer period. Due to the rotation mechanism of VBS, the elements in $B_{\text{HB-2}}(k-1)$ are more likely to exit the $A_{\text{HB-2}}(k-1)$ than the elements not in $B_{\text{HB-2}}(k-1)$ [28]. Therefore, the second subset accounts for a lower proportion than the first subset. When the second subset accounts for the same proportion as the first subset, the $N_{\text{HB-sw2-sum}}(p)$ takes the value as $2N_{\text{HB-2}}$ in this article. Based on the above analysis, if the $N_{\text{HB-2th}}$ is selected too lower, $N_{\text{HB-sw2-sum}}(p)$ may exceed $N_{\text{HB-2th}}$ before the $B_{\text{HB-2}}(p)$ becomes an empty set when no IGBT OCFs occur, which means the diagnostic process may mistake normal SM as the faulty SM. To avoid misdiagnosis, $N_{\text{HB-2th}}$ is selected as two times of $N_{\text{HB-2}}$ in this article. It should to be emphasized that the selection of threshold in this article may not be the optimal choice since the optimal selection for the threshold is hard to determine. However, the threshold selected in this article, which is based on both theory and experience, is capable of guaranteeing the effectiveness of the proposed strategy in our scenario. All diagnostic methods in Fig. 16 follow this principle when selecting the thresholds.

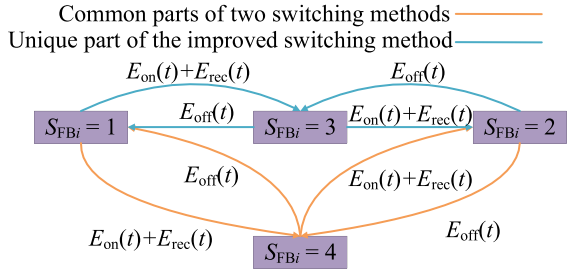

Fig. 18. Comparisons of switching losses when arm current is positive.

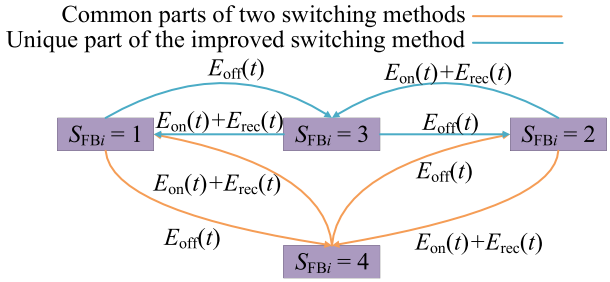

Fig. 19. Comparisons of switching losses when arm current is negative.

VII. Further Discussion of the Proposed Improved Switching Method and the Diagnostic Strategy

A. Comparisons of the Switching Losses Between the Two Switching Methods

The existing switching method only uses Mode 4 and Mode 8 as the bypassed state for the consideration of switching loss. However, the proposed improved switching method remains the switching loss unchanged compared to the existing switching method. The switching losses between these two switching methods are compared in detail as follows.

According to paper [11], switching losses in the FBSM are composed of three main parts: the turn-ON loss of IGBT $E_{\rm on}(t)$, the turn-OFF loss of IGBT $E_{\rm off}(t)$, and the reverse recovery loss of diode $E_{\rm rec}(t)$. $E_{\rm on}(t)$, $E_{\rm off}(t)$, and $E_{\rm rec}(t)$ are all functions relative to time [11]. To simplify the analysis, it is assumed that all IGBTs and diodes generate the same switching losses. Therefore, switching losses in the FBSM are relevant to two indices. The first index is the switching moment of the switching sequence, which depends on the control period and the adopted VBS. The proposed improved switching method is not related to the control period or the adopted VBS and therefore does not affect the switching moment of the switching sequence. The second index pertains to the devices involved in each switching moment of the switching sequence, which will be discussed as follows.

For the existing switching method, if $S_{{\rm FB}i}$ needs to switch from 1 to 4 and the arm current is positive, $\rm D_1$ turns OFF and $\rm T_2$ turns ON, thus generating $E_{\rm on}(t)$ and $E_{\rm rec}(t)$, respectively. If $S_{{\rm FB}i}$ needs to switch from 4 to 1 and the arm current is positive, $\rm D_1$ turns ON and $\rm T_2$ turns OFF, thus generating $E_{\rm off}(t)$ correspondingly. If $S_{{\rm FB}i}$ needs to switch from 2 to 4 and the arm current is positive, $\rm D_4$ turns ON and $\rm T_3$ turns OFF, thus generating $E_{\rm off}(t)$, respectively. If $S_{{\rm FB}i}$ needs to switch from 4 to 2 and the arm current is positive, $\rm D_4$ turns OFF and $\rm T_3$ turns ON, thus generating $E_{\rm on}(t)$ and $E_{\rm rec}(t)$, respectively. Based on the analysis, the switching losses of the existing switching method when the arm current is positive $E_{\text{exi-pos}}(t)$ can be expressed as (18) and shown in Fig. 18

$$E_{\rm exi-pos}(t)=\begin{cases}E_{\rm on}(t)+E_{\rm rec}(t), & S_{{\rm FB}i}=1\rightarrow S_{{\rm FB}i}=4\\ E_{\rm off}(t), & S_{\rm FBi}=4\rightarrow S_{{\rm FB}i}=1\\ E_{\rm off}(t), & S_{\rm FBi}=2\rightarrow S_{{\rm FB}i}=4\\ E_{\rm on}(t)+E_{\rm rec}(t), & S_{{\rm FB}i}=4\rightarrow S_{{\rm FB}i}=2.\end{cases}\tag{18}$$

Similarly, the switching losses of the existing switching method when the arm current is negative $E_{\text{exi-neg}}(t)$ can be expressed as (19) and shown in Fig. 19

$$E_{\rm exi-neg}(t)=\begin{cases}E_{\rm off}(t), & S_{{\rm FB}i}=1\rightarrow S_{{\rm FB}i}=4\\ E_{\rm on}(t)+E_{\rm rec}(t), & S_{{\rm FB}i}=4\rightarrow S_{{\rm FB}i}=1\\ E_{\rm on}(t)+E_{\rm rec}(t), & S_{{\rm FB}i}=2\rightarrow S_{{\rm FB}i}=4\\ E_{\rm off}(t), & S_{{\rm FB}i}=4\rightarrow S_{{\rm FB}i}=2.\end{cases}\tag{19}$$

The proposed improved switching method has the same switching losses as the existing switching method when $S_{{\rm FB}i}$ switches between 1 and 4 or 2 and 4. Compared to the existing switching method, the proposed switching method adds the switching processes of $S_{{\rm FB}i}$ between 1 and 3 or 2 and 3. If $S_{{\rm FB}i}$ needs to switch from 1 to 3 and the arm current is positive, $\rm D_4$ turns OFF and $\rm T_3$ turns ON, thus generating $E_{\rm on}(t)$ and $E_{\rm rec}(t)$, respectively. If $S_{{\rm FB}i}$ needs to switch from 3 to 1 and the arm current is positive, $\rm D_4$ turns ON and $\rm T_3$ turns OFF, thus generating $E_{\rm off}(t)$ correspondingly. If $S_{{\rm FB}i}$ needs to switch from 2 to 3 and the arm current is positive, $\rm D_1$ turns ON and $\rm T_2$ turns OFF, thus generating $E_{\rm off}(t)$ correspondingly. If $S_{{\rm FB}i}$ needs to switch from 3 to 2 and the arm current is positive, $\rm D_1$ turns OFF and $\rm T_2$ turns ON, thus generating $E_{\rm on}(t)$ and $E_{\rm rec}(t)$, respectively. Based on the analysis, the switching losses of the proposed improved switching method when the arm current is positive $E_{\text{pro-pos}}(t)$ can be expressed as (20) and shown in Fig. 18

$$E_{\rm pro-pos}(t)=\begin{cases}E_{\rm on}(t)+E_{\rm rec}(t), & S_{{\rm FB}i}=1\rightarrow S_{{\rm FB}i}=3/4\\ E_{\rm off}(t), & S_{{\rm FB}i}=3/4\rightarrow S_{{\rm FB}i}=1\\ E_{\rm off}(t), & S_{{\rm FB}i}=2\rightarrow S_{{\rm FB}i}=3/4\\ E_{\rm on}(t)+E_{\rm rec}(t), & S_{{\rm FB}i}=3/4\rightarrow S_{{\rm FB}i}=2.\end{cases}\tag{20}$$

Similarly, the switching losses of the improved switching method when the arm current is negative $E_{\text{pro-neg}}(t)$ can be expressed as (21) and shown in Fig. 19

$$E_{\rm pro-neg}(t)=\begin{cases}E_{\rm off}(t), & S_{{\rm FB}i}=1\rightarrow S_{{\rm FB}i}=3/4\\ E_{\rm on}(t)+E_{\rm rec}(t), & S_{{\rm FB}i}=3/4\rightarrow S_{{\rm FB}i}=1\\ E_{\rm on}(t)+E_{\rm rec}(t), & S_{{\rm FB}i}=2\rightarrow S_{{\rm FB}i}=3/4\\ E_{\rm off}(t), & S_{{\rm FB}i}=3/4\rightarrow S_{{\rm FB}i}=2.\end{cases}\tag{21}$$

According to (3), when $S_{{\rm Fun\text{-}FB}i}$ needs to switch between 1 and 0, $S_{{\rm FB}i}$ needs to switch between 1 and 4 under the existing switching method, while $S_{{\rm FB}i}$ needs to switch between 1 and

3 or 1 and 4 based on $F_{\mathrm{FB}i}$ under the improved switching method. Based on (20) and (21), the switching losses of $S_{\mathrm{FB}i}$ when switching between 1 and 4 are equivalent to those when switching between 1 and 3. According to (3), when $S_{\mathrm{Fun\text{-}FB}i}$ needs to switch between -1 and 0, $S_{\mathrm{FB}i}$ needs to switch between 2 and 4 under the existing switching method, while $S_{\mathrm{FB}i}$ needs to switch between 2 and 3 or 2 and 4 based on $F_{\mathrm{FB}i}$ under the improved switching method. Based on (20) and (21), the switching losses of $S_{\mathrm{FB}i}$ when switching between 2 and 4 are equivalent to those when switching between 2 and 3. Therefore, it can be verified that the improved switching method remains the switching loss unchanged compared to the existing switching method. Combining the analysis in Section IV-C with this section, it is demonstrated that the proposed switching method can thoroughly exhibit the fault characteristics of IGBT OCFs without adding extra switching losses.

B. Range of Application

According to papers [4] and [10], HMMCs, HBMMCs, and FBMMCs all operate in the same way during Part I and Part IV. Since the diagnostic targets of both Part I and Part IV encompass two types of faults within the HBSM and all four types of faults within the FBSM, it is confirmed that the proposed ISM-based diagnostic strategy is applicable to HBMMCs and FBMMCs as well.

C. Performance of the Proposed Diagnostic Strategy When the HMMC Operates Under Reduced DC Voltage or Rated DC Voltage

As indicated in Section IV-C, only Part I, Part III, and Part IV exist when the HMMC operates in the rectifier mode under reduced dc voltage. In this sense, the proposed strategy corresponding to Part II in Fig. 16 is not activated. However, the existing three parts contain all six types of IGBT OCFs based on Fig. 14. Therefore, the proposed strategy can diagnose all six types of IGBT OCFs in HMMCs effectively under such operation conditions by activating the appropriate methods in each part. When the MMC operates in the inverter mode under reduced dc voltage, only Part I, Part II, and Part IV exist. In this sense, the proposed strategy corresponding to Part III in Fig. 16 is not activated. However, the existing three parts contain all six types of IGBT OCFs based on Fig. 14. Therefore, the proposed strategy can also diagnose all six types of IGBT OCFs in HMMCs effectively under such operation conditions.

As indicated in Section II-B, there exists $M_{\mathrm{ac}} < 1$ and $M_{\mathrm{dc}} = 1$ when the HMMC operates under rated dc voltage. Therefore, it can be obtained from (11) that u_{arm} is always positive, which means the arm need not generate negative voltage. According to paper [27], regardless of whether the MMC operates in rectifier mode or inverter mode, it always contains Part I and Part IV. It can be observed from Fig. 14 that Part I and Part IV also contain all six types of IGBT OCFs. Therefore, the proposed strategy can diagnose all six types of IGBT OCFs in HMMCs effectively under such operation conditions.

Based on the above analysis, the proposed diagnostic strategy can diagnose all types of IGBT OCFs effectively under different dc voltage levels.

D. Performance of the Proposed Diagnostic Strategy Under Load Change

Due to the VBS, the capacitor voltages of the same type SMs in the arms are still well-balanced when the load changes. Therefore, the switching sequences of the normal SMs with the same type still have consistent trends. In particular, the switching sequences of normal SMs with the same type are all in the state of dynamic change in most cases or all remaining at a specific value in special cases. Since an SM is diagnosed as a faulty SM only if the SM remains in a specific sequence for a period of time while the switching sequences of other SMs with the same type are still dynamically changing, the proposed diagnostic strategy does not mistake normal SMs as faulty SMs during load change.

Furthermore, since the trends of switching sequences in the normal SMs have few differences under different loads, the diagnostic threshold is insensitive to load changes [28]. Therefore, the proposed diagnostic strategy works effectively under different loads without readjusting the diagnostic thresholds.

E. Performance of the Proposed Diagnostic Strategy Under DC-Side Fault

According to papers [11], [29], and [30], the main advantage of HMMC is its ability to actively ride-through dc-side faults, the performance of the proposed diagnostic strategy under dc-side fault is discussed in this section.

When a dc-side short-circuit fault occurs, the SM capacitor voltages change. However, the capacitor voltage deviation between the same type SMs in the arm can still be controlled due to the VBS, thus the capacitor voltages of the same type SMs have an overall offset. Therefore, the switching sequences of the normal SMs with the same type still have consistent trends. In particular, the switching sequences of normal SMs with the same type are all in the state of dynamic change in most cases or all remaining at a specific value in special cases. Since an SM is diagnosed as a faulty SM only if the SM remains in a specific sequence for a period of time while the switching sequences of other SMs with the same type are still dynamically changing, the proposed diagnostic strategy does not mistake normal SMs as the faulty SM during dc faults.

F. Impact of the IGBT Switching Frequency on the Speed and Performance of the Proposed Diagnostic Strategy

Taking the diagnostic process of identifying the Type $\mathrm{II}_{\mathrm{HB}}$ malfunctioning SM in Part I as an example to illustrate how the IGBT switching frequency affects the speed and performance of the proposed strategy.

In order for the Type $\mathrm{II}_{\mathrm{HB}}$ malfunctioning SM to be identified in Part I, two conditions must be met concurrently. The first condition is that the faulty SM is included in $B_{\mathrm{HB\text{-}2}}$ monitored by the diagnostic process. The second condition is that $N_{\mathrm{HB\text{-}sw2\text{-}sum}}$

exceeds $N_{\text{HB-2th}}$ in Part I. Therefore, the time taken to diagnose the Type II_{HB} malfunctioning SM can be expressed as follows:

$$t_{\text{d-IIHB}} = t_{\text{I}} + t_{\text{II}} \tag{22}$$

where t_{I} represents the time taken for the faulty SM to be included in $B_{\text{HB-2}}$ and t_{II} represents the time taken for $N_{\text{HB-sw2-sum}}$ to exceed $N_{\text{HB-2th}}$.

If the faulty SM is initially included in $B_{\text{HB-2}}$, t_{I} is 0. If the initial switching sequence of the faulty SM is 1, it should switch to 2 to be included in $B_{\text{HB-2}}$. The lower the IGBT switching frequency f_{sw}, the slower the switch of the SM switching sequence is. Therefore, the time taken for the switching sequence of the faulty SM to switch from 1 to 2 is longer when the f_{sw} is lower. In other words, a lower f_{sw} results in a longer t_{I}.

For t_{II}, it depends on the growth rate of $N_{\text{HB-sw2-sum}}$. The lower the f_{sw}, the slower the switch of the SM switching sequence is. Therefore, the lower the f_{sw}, the slower the growth rate of $N_{\text{HB-sw2-sum}}$ is. In other words, a lower f_{sw} results in a longer t_{II}. When the f_{sw} is too low, $t_{\text{d-IIHB}}$ may exceed the time of a single part and result in a delay in the diagnostic process of more than one part.

Based on the above analysis, it can be concluded that the IGBT switching sequency affects the speed and the performance of the proposed strategy: the lower the IGBT switching frequency, the slower the speed of the proposed strategy is. In particular, if the IGBT switching frequency is too low, this may result in a delay in the diagnostic process of more than one part. Therefore, the proposed diagnostic strategy is not recommended for applications where the IGBT switching frequency is too low.

VIII. Experimental Verification

As a consequence of the restricted number of SMs in the reduced-scale MMC prototype, it is difficult for the scaled-down prototype to demonstrate the working process of the proposed diagnostic strategy well. The HIL platform represents the optimal choice for the verification in this article, given its frequent utilization in multiple similar studies. Therefore, a HIL platform is constructed in our lab, as shown in Fig. 20. Therein, the power-stage model of an HMMC in Fig. 1 is first built and compiled on the host machine. Subsequently, it is downloaded to the Advantech IPC-610L target machine for real-time simulation. The conversion and communication of the signals between the target machine and the DSP control board are realized by an I/O card. The oscilloscope enables real-time monitoring of the experimental waveforms. Table IV lists the parameters adopted by the HMMC.

A. Verification of the Proposed Improved Switching Method in FBSM

To verify the effectiveness of the proposed improved switching method, experiments under the proposed switching method and the existing switching method are both conducted. Experimental waveforms of two switching methods are shown in Fig. 21, where $S_{\text{auFB1-pro}}$ and $S_{\text{auFB1-ori}}$ represent the switching sequence of the SM with sequence number 1 under the proposed improved switching method and the existing switching method,

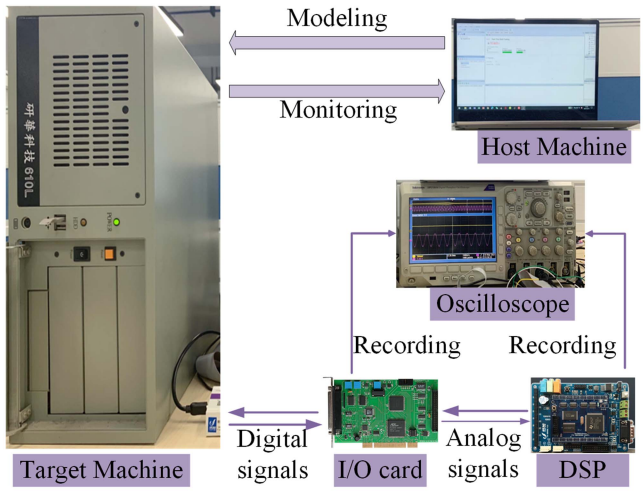

Fig. 20. Photograph of the HIL platform.

TABLE IV
Experimental Parameters

Parameters	Value
AC side rated voltage	290 kV
AC side voltage frequency	50 Hz
DC side rated voltage	500 kV
Rated active power	750 MW
Number of FBSMs per arm	160
Number of HBSMs per arm	84
Arm inductance	0.1 H
SM capacitance	8 mF
DC modulation index	0.8

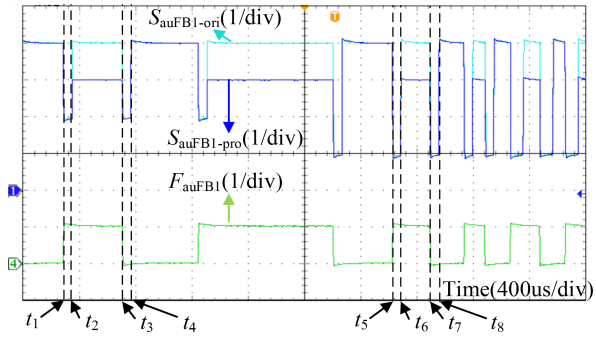

Fig. 21. Experimental waveforms of the proposed improved switching method and the existing switching method.

respectively. F_{auFB1} represents the flag for the bypassed switching sequence selection of the SM with sequence number 1.

At time t_1, $S_{\text{auFB1-ori}}$ switches from 4 to 2, indicating that the SM needs to switch from the bypassed state to the negatively inserted state. Thus, F_{auFB1} is negated at this moment, which aligns with the flowchart of the proposed switching method. Then, $S_{\text{auFB1-ori}}$ switches from 2 to 4 at time t_2, indicating that the SM needs to switch from the negatively inserted state to the bypassed state. Since F_{auFB1} equals 1 at this moment, $S_{\text{auFB1-pro}}$ switches from 2 to 3, which aligns with the proposed switching method. Similar to t_1, F_{auFB1} is negated again at t_3.

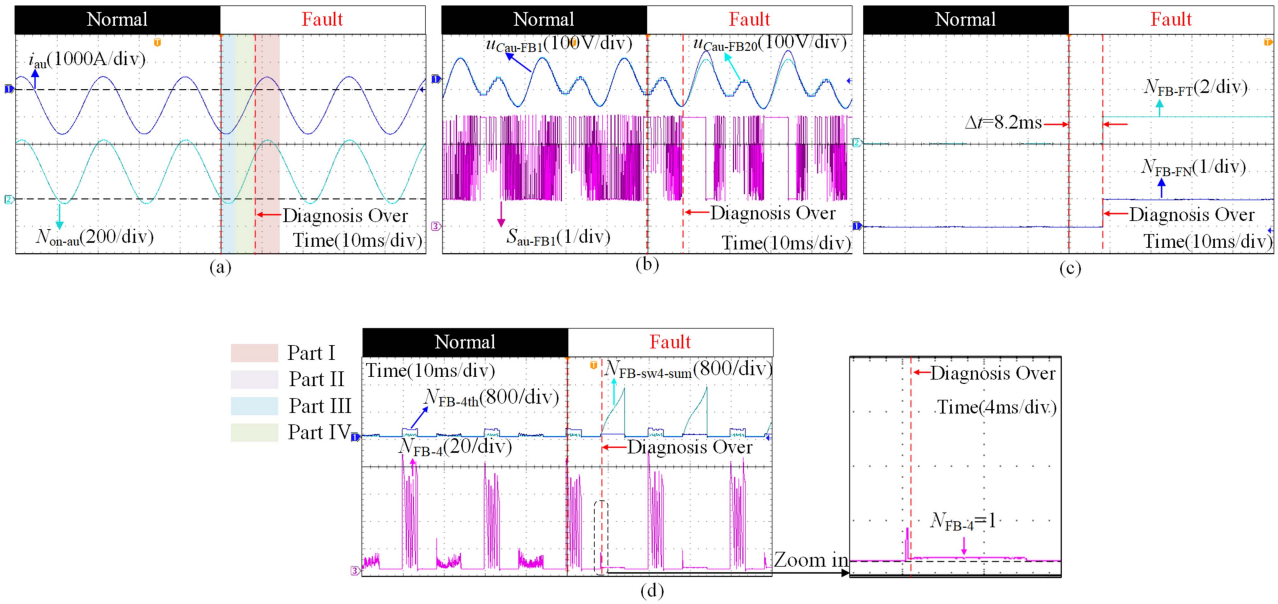

Fig. 22. Experimental waveforms of experiment I.A. (a) Arm current and number of inserted SMs. (b) SM capacitor voltages and switching sequence. (c) Type and sequence number of faulty SM. (d) Relevant variables in the diagnostic method of identifying the FBSM whose S_{FBi} remains at 4.

TABLE V
EXPERIMENTAL SCENARIOS

Number	Part to be verified	Faults
I. A	I	A Type II_{FB} fault
I. B	I	A Type III_{FB} fault
I. C	I	A Type II_{HB} fault
II	II	A Type II_{FB} fault and a Type III_{FB} fault
III. A	III	A Type I_{FB} fault
III. B	III	A Type IV_{FB} fault
IV. A	IV	A Type I_{FB} fault and a Type IV_{FB} fault
IV. B	IV	A Type I_{HB} fault

Then $S_{\text{auFB1-pro}}$ switches from 2 to 4 at t_4 because F_{auFB1} equals 0 at this moment, which aligns with the proposed switching method. Based on the above analysis, it is demonstrated that the proposed improved switching method can function correctly when N_{on} is negative. The effectiveness of the proposed ISM when N_{on} is positive can be proved at t_5, t_6, t_7, and t_8, whose analytical process is similar to that when N_{on} is negative. Moreover, it can be observed from Fig. 21 that the proposed switching method does not affect the switching moment of the switching sequence. Combining the analysis in Section IV-B with the experimental verification in this section, it can be concluded that the proposed improved switching method keeps the switching loss unchanged compared to the existing switching method.

B. Verification of the Proposed Fault Diagnostic Strategy

To verify the effectiveness of the proposed diagnostic strategy, it is only necessary to verify that the proposed strategy works effectively in all four parts. Therefore, the experimental scenarios are considered based on Figs. 14 and 16, as listed in Table V. The part to be verified in Table V represents the part of the proposed strategy that is to be verified for effectiveness in the corresponding experimental scenario. It should be emphasized that the reason for setting up two types of faults in Experiment II and Experiment IV. A is that both two types of faults have the same switching sequence characteristics in the corresponding part. Moreover, such a setup also verifies that the proposed diagnostic strategy can handle cases where multiple faults exist in the arm simultaneously.

1) Experiment I. A: Experimental waveforms of Experiment I. A are shown in Fig. 22. To improve the display of SM capacitor voltage in the oscilloscope, the dc bias U_{dc}/N is subtracted from the SM capacitor voltage. The meaning of $N_{\text{FB-FT}}$ is defined as the following equations to better reflect the diagnostic results:

$$N_{\text{FB-FT}} = \begin{cases} 1, & \text{Type } I_{FB} \text{ fault} \\ 2, & \text{Type } II_{FB} \text{ fault} \\ 3, & \text{Type } III_{FB} \text{ fault} \\ 4, & \text{Type } IV_{FB} \text{ fault} \\ 5, & \text{Type } I_{FB}/IV_{FB} \text{ fault} \\ 6, & \text{Type } II_{FB}/III_{FB} \text{ fault.} \end{cases} \tag{23}$$

As shown in Fig. 22(a), the Type II_{FB} fault occurs during Part III. Therefore, the Type II_{FB} fault cannot exhibit fault characteristics immediately. Upon entering Part I, the Type II_{FB} fault can exhibit fault characteristics. As shown in Fig. 22(b), the switching sequence of the Type II_{FB} faulty SM remains at 4 during Part I, which is consistent with the previous analysis in Section V-B. Therefore, the faulty SM can be diagnosed by the diagnostic method of identifying the FBSM whose S_{FBi} remains at 4 during Part I. As shown in Fig. 22(d), $N_{\text{FB-sw4-sum}}$ increases continuously and eventually exceeds $N_{\text{FB-4th}}$. From the zoom-in figure of Fig. 22(d), $N_{\text{FB-4}}$ equals 1 when the threshold is exceeded, which indicates that a Type II_{FB} faulty SM is identified through the diagnostic method. As shown in Fig. 22(c), $N_{\text{FB-FT}}$ is 2 and $N_{\text{FB-FN}}$ is 1, which represents the sequence number and the faulty type of the faulty SM correctly. The diagnosis takes

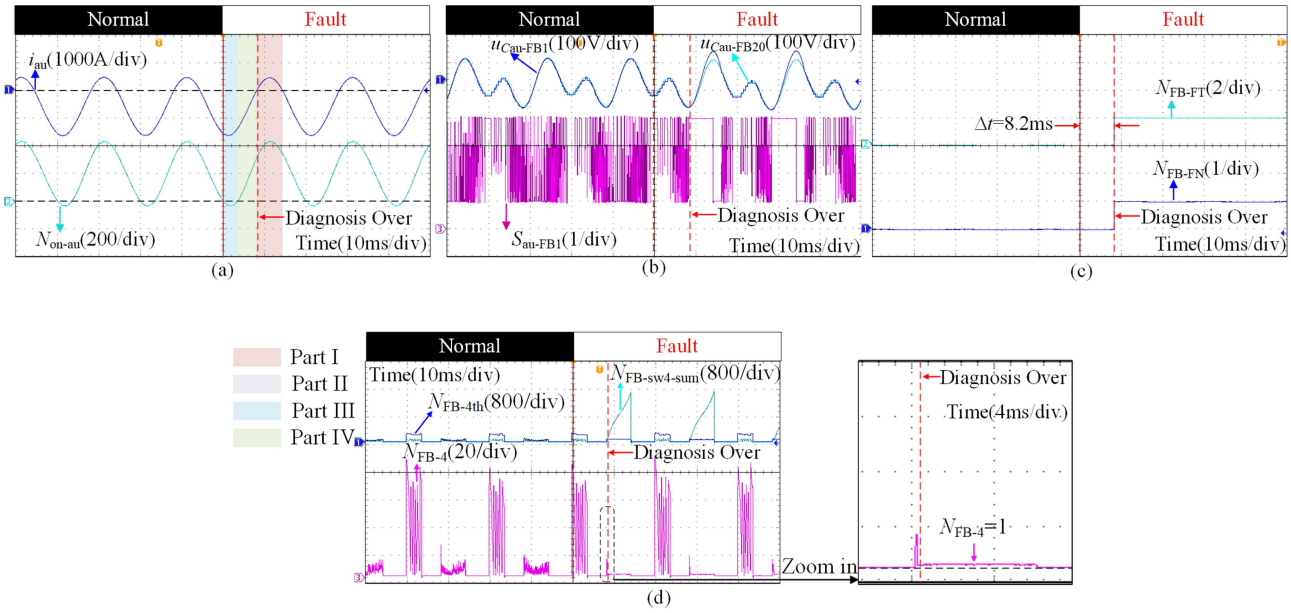

Fig. 23. Experimental waveforms of experiment I.B. (a) Arm current and number of inserted SMs. (b) SM capacitor voltages and switching sequence. (c) Type and sequence number of faulty SM. (d) Relevant variables in the diagnostic method of identifying the FBSM whose S_{FBi} remains at 3.

8.2 ms. Based on the above analysis, the proposed diagnostic strategy can diagnose Type II_{FB} fault correctly in Part I.

2) Experiment I. B: Experimental waveforms of Experiment I. B are shown in Fig. 23. As shown in Fig. 23(a), the Type III_{FB} fault occurs during Part III. Therefore, the Type III_{FB} fault cannot exhibit fault characteristics immediately. Upon entering Part I, the Type III_{FB} fault can exhibit fault characteristics. As shown in Fig. 23(b), the switching sequence of the Type III_{FB} faulty SM remains at 3 during Part I, which is consistent with the previous analysis in Section V-B. Therefore, the faulty SM can be diagnosed by the diagnostic method of identifying the FBSM whose S_{FBi} remains at 3 during Part I. As shown in Fig. 23(d), $N_{\text{FB-sw3-sum}}$ increases continuously and eventually exceeds $N_{\text{FB-3th}}$. From the zoom-in figure of Fig. 23(d), $N_{\text{FB-3}}$ equals 1 when the threshold is exceeded, which indicates that a Type III_{FB} faulty SM is identified through the diagnostic method. As shown in Fig. 23(c), $N_{\text{FB-FT}}$ is 3 and $N_{\text{FB-FN}}$ is 1, which represents the sequence number and the faulty type of the faulty SM correctly. The diagnosis takes 8.6 ms. Based on the above analysis, the proposed diagnostic strategy can diagnose Type III_{FB} fault correctly in Part I.

3) Experiment I. C: Experimental waveforms of Experiment I. B are shown in Fig. 24. The meaning of $N_{\text{HB-FT}}$ is defined as the following equations to better reflect the diagnostic results:

$$N_{\text{HB-FT}} = \begin{cases} 1, & \text{Type } \text{I}_{\text{HB}} \text{ fault} \\ 2, & \text{Type } \text{II}_{\text{HB}} \text{ fault} \end{cases}. \tag{24}$$

As shown in Fig. 24(a). the Type II_{HB} fault occurs during Part III. Therefore, the Type II_{HB} fault cannot exhibit fault characteristics immediately. Upon entering Part I, the Type II_{HB} fault can exhibit fault characteristics. As shown in Fig. 24(b), the switching sequence of the Type II_{HB} faulty SM remains at 2 during Part I, which is consistent with the previous analysis in Section V-B. Therefore, the faulty SM can be diagnosed by the diagnostic method of identifying the HBSM whose S_{HBi} remains at 2 during Part I. As shown in Fig. 24(d), $N_{\text{HB-sw2-sum}}$ increases continuously and eventually exceeds $N_{\text{HB-2th}}$. From the zoom-in figure of Fig. 24(d), $N_{\text{HB-2}}$ equals 1 when the threshold is exceeded, which indicates that a Type II_{HB} faulty SM is identified through the diagnostic method. As shown in Fig. 24(c), $N_{\text{HB-FT}}$ is 2 and $N_{\text{HB-FN}}$ is 1, which represents the sequence number and the faulty type of the faulty SM correctly. The diagnosis takes 8.5 ms. Based on the above analysis, the proposed diagnostic strategy can diagnose Type III_{FB} fault correctly in Part I.

4) Experiment II: Experimental waveforms of Experiment II is shown in Fig. 25. As shown in Fig. 25(a), the Type II_{FB} fault and the Type III_{FB} fault occur during Part II. Therefore, both two faults can exhibit their fault characteristics immediately as shown in Fig. 25(b) and (c). The capacitor voltages of malfunctioning SMs remain unchanged during Part II as shown in Fig. 25(b). As shown in Fig. 25(c), the switching sequences of the Type II_{FB} faulty SM and the Type III_{FB} faulty SM both remain at 2 during Part II, which is consistent with the previous analysis in Section V-B. Therefore, the faulty SMs can be diagnosed by the diagnostic method of identifying the FBSM whose S_{FBi} remains at 2 during Part II. As shown in Fig. 25(d), $N_{\text{FB-sw2-sum}}$ increases continuously and eventually exceeds $N_{\text{FB-2th}}$ and $N_{\text{FB-2}}$ equals 1 when the threshold is exceeded, which indicates that two faulty SMs are identified through the diagnostic method. As shown in Fig. 25(e) and (f), $N_{\text{FB-FN1}}$ is 1, $N_{\text{FB-FN2}}$ is 2, $N_{\text{FB-FT1}}$ is 6, and $N_{\text{FB-FT2}}$ is 6, which represent the sequence numbers and the faulty types of two faulty SMs correctly. The diagnosis takes 0.3 ms. It should be noted that the proposed diagnostic strategy cannot identify whether they are Type II_{FB} faults or Type III_{FB}

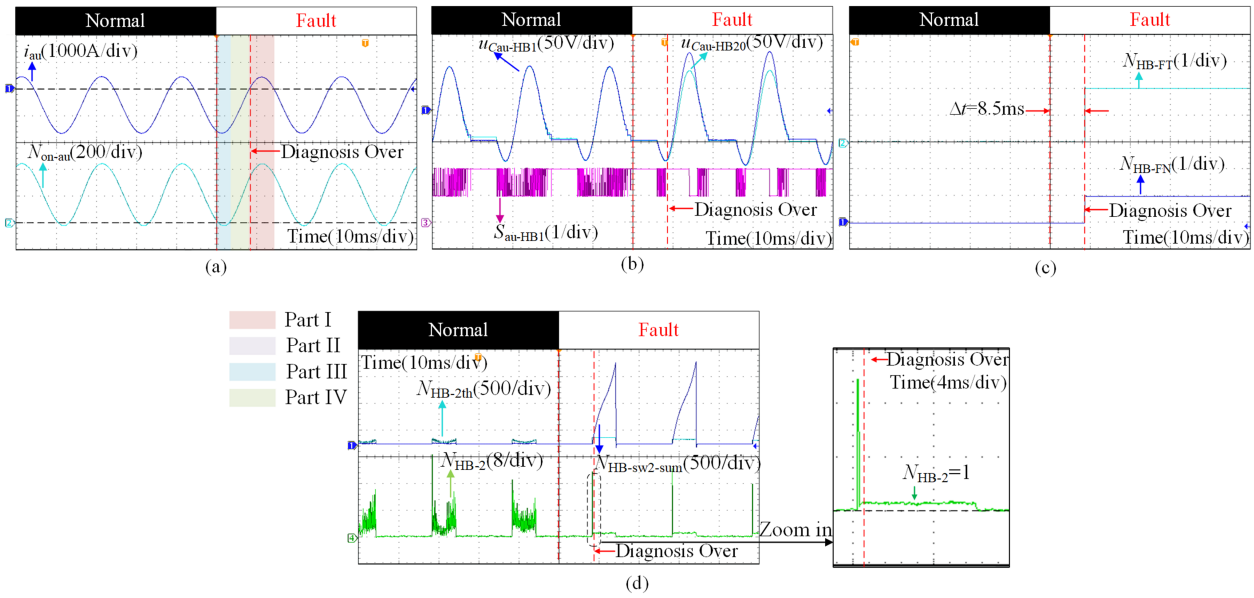

Fig. 24. Experimental waveforms of experiment I.C. (a) Arm current and number of inserted SMs. (b) SM capacitor voltages and switching sequence. (c) Type and sequence number of faulty SM. (d) Relevant variables in the diagnostic method of identifying the HBSM whose $S_{\mathrm{HB}i}$ remains at 2.

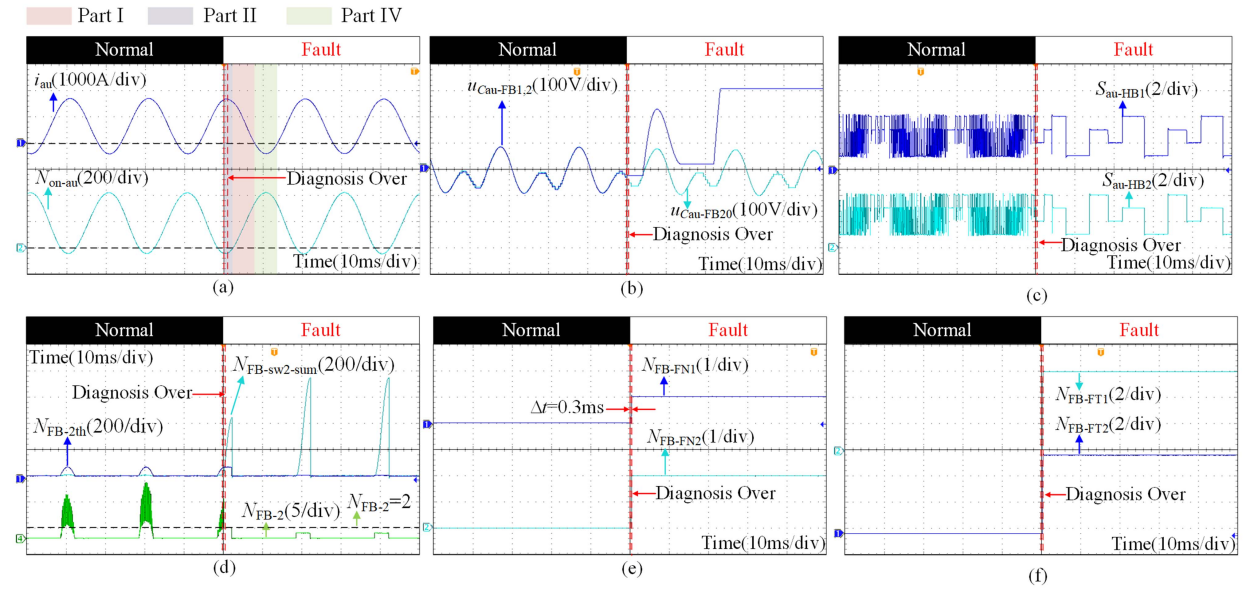

Fig. 25. Experimental waveforms of experiment II. (a) Arm current and number of inserted SMs. (b) SM capacitor voltage. (c) SM switching sequence. (d) Relevant variables in the diagnostic method of identifying the FBSM whose $S_{\mathrm{FB}i}$ remains at 2. (e) Sequence numbers of faulty SMs. (f) Faulty types of faulty SMs.

faults because both two faults share the same switching sequence characteristics in Part II. Based on the above analysis, the proposed diagnostic strategy can diagnose Type $\mathrm{II}_{\mathrm{FB}}$ fault and Type $\mathrm{III}_{\mathrm{FB}}$ fault correctly in Part II.

5) Experiment III. A: Experimental waveforms of Experiment III. A are shown in Fig. 26. As shown in Fig. 26(a), the Type I_{FB} fault occurs during Part III. Therefore, the Type I_{FB} fault can exhibit fault characteristics immediately. As shown in Fig. 26(b), the switching sequence of the Type I_{FB} faulty SM remains at 3 during Part III, which is consistent with the previous analysis in Section V-B. Therefore, the faulty SM can be diagnosed by the diagnostic method of identifying the FBSM whose $S_{\mathrm{FB}i}$ remains at 3 during Part III. As shown in Fig. 26(d), $N_{\mathrm{FB\text{-}sw3\text{-}sum}}$ increases continuously and eventually exceeds $N_{\mathrm{FB\text{-}3th}}$. From the zoom-in figure of Fig. 26(d), $N_{\mathrm{FB\text{-}3}}$ equals 1 when the threshold is exceeded, which indicates that a Type I_{FB} faulty SM is identified through the diagnostic method. As shown in Fig. 26(c), $N_{\mathrm{FB\text{-}FT}}$ is 1 and $N_{\mathrm{FB\text{-}FN}}$ is 1, which represents the sequence number and the faulty type of the faulty SM correctly. The diagnosis takes 2.4 ms. Based on the above analysis, the proposed diagnostic strategy can diagnose Type I_{FB} fault correctly in Part III.

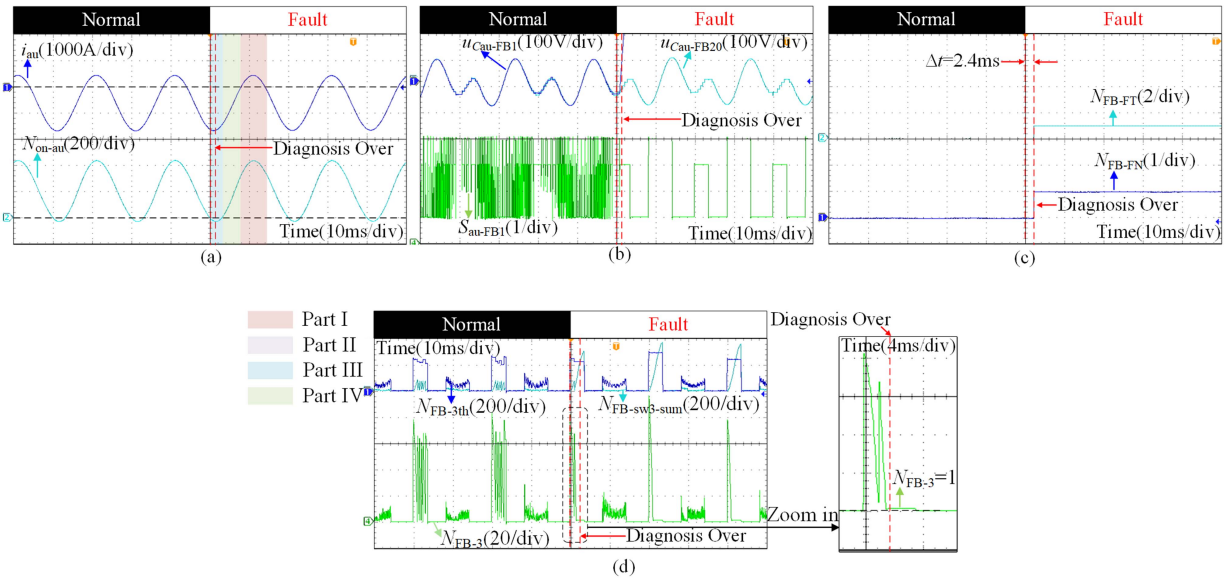

Fig. 26. Experimental waveforms of experiment III.A. (a) SM capacitor voltage and switching sequence. (b) Arm current and number of inserted SMs. (c) Type and sequence number of faulty SM. (d) Relevant variables in the diagnostic method of identifying the FBSM whose $S_{\mathrm{FB}i}$ remains at 3.

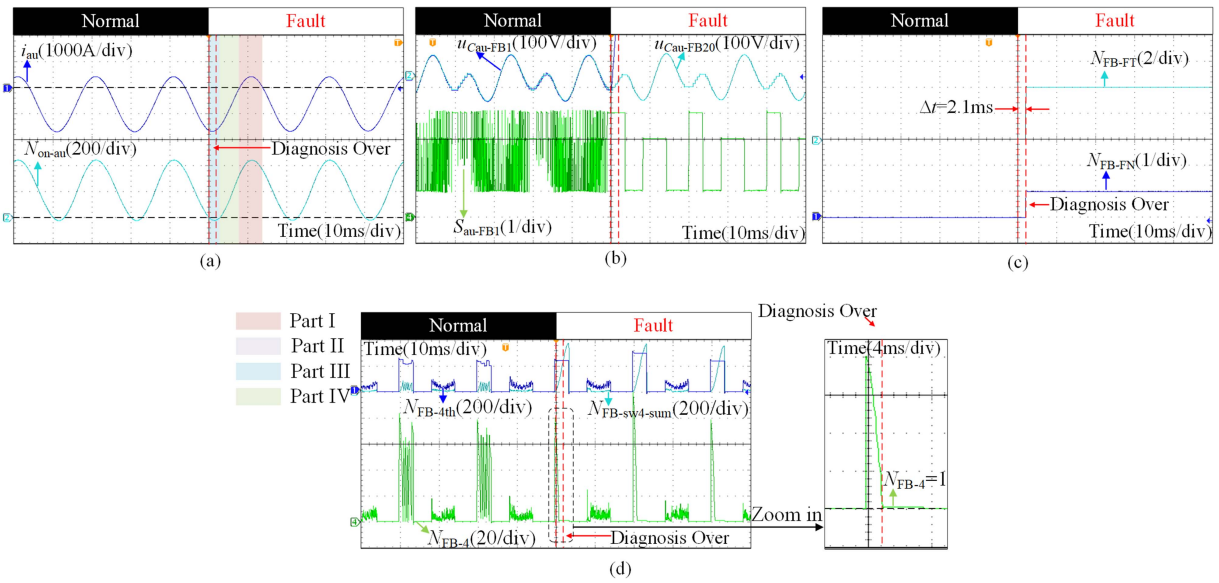

Fig. 27. Experimental waveforms of experiment III.B. (a) SM capacitor voltage and switching sequence. (b) Arm current and number of inserted SMs. (c) Type and sequence number of faulty SM. (d) Relevant variables in the diagnostic method of identifying the FBSM whose $S_{\mathrm{FB}i}$ remains at 4.

6) Experiment III. B: Experimental waveforms of Experiment III. B are shown in Fig. 27. As shown in Fig. 27(a). the Type $\mathrm{IV_{FB}}$ fault occurs during Part III. Therefore, the Type $\mathrm{IV_{FB}}$ fault can exhibit fault characteristics immediately. As shown in Fig. 27(b), the switching sequence of the Type $\mathrm{IV_{FB}}$ faulty SM remains at 4 during Part III, which is consistent with the previous analysis in Section V-B. Therefore, the faulty SM can be diagnosed by the diagnostic method of identifying the FBSM whose $S_{\mathrm{FB}i}$ remains at 4 during Part III. As shown in Fig. 27(d), $N_{\mathrm{FB\text{-}sw4\text{-}sum}}$ increases continuously and eventually exceeds $N_{\mathrm{FB\text{-}4th}}$. From the zoom-in figure of Fig. 27(d), $N_{\mathrm{FB\text{-}4}}$ equals 1 when the threshold is exceeded, which indicates that a Type $\mathrm{IV_{FB}}$ faulty SM is identified through the diagnostic method. As shown in Fig. 27(c), $N_{\mathrm{FB\text{-}FT}}$ is 4 and $N_{\mathrm{FB\text{-}FN}}$ is 1, which represents the sequence number and the faulty type of the faulty SM correctly. The diagnosis takes 2.1 ms. Based on the above analysis, the proposed diagnostic strategy can diagnose Type $\mathrm{IV_{FB}}$ fault correctly in Part III.

7) Experiment IV. A: Experimental waveforms of Experiment I. B are shown in Fig. 28. As shown in Fig. 28(a). the Type

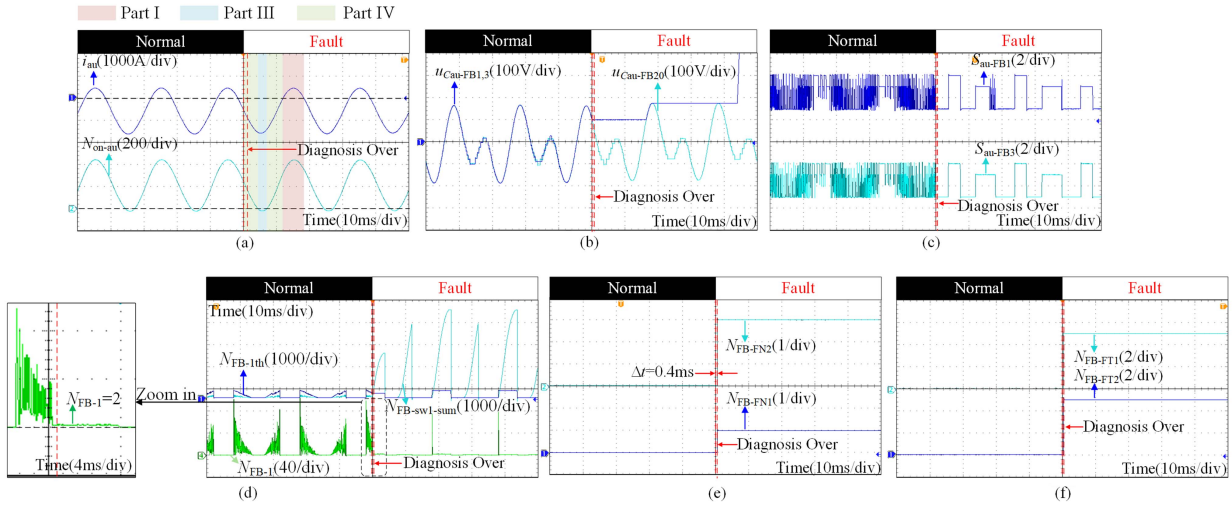

Fig. 28. Experimental waveforms of experiment IV.A. (a) Arm current and number of inserted SMs. (b) SM capacitor voltage. (c) SM switching sequence. (d) Relevant variables in the diagnostic method of identifying the FBSM whose $S_{\mathrm{FB}i}$ remains at 1. (e) Sequence numbers of faulty SMs. (f) Faulty types of faulty SMs.

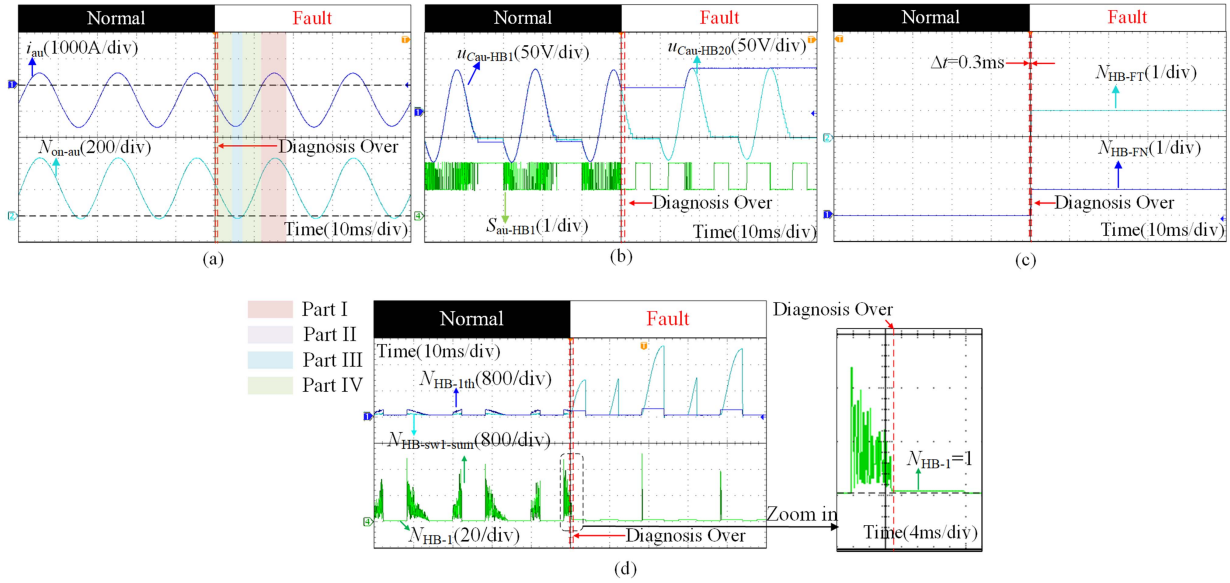

Fig. 29. Experimental waveforms of experiment IV.B. (a) Arm current and number of inserted SMs. (b) SM capacitor voltage and switching sequence. (c) Type and sequence number of faulty SM. (d) Relevant variables in the diagnostic method of identifying the HBSM whose $S_{\mathrm{HB}i}$ remains at 1.

I_{FB} fault and Type $\mathrm{IV}_{\mathrm{FB}}$ fault occur during Part IV. Therefore, the Type I_{FB} fault and Type $\mathrm{IV}_{\mathrm{FB}}$ fault can exhibit fault characteristics immediately. As shown in Fig. 28(b), the capacitor voltages of both two malfunctioning SMs remain unchanged during Part IV. As shown in Fig. 28(c), the switching sequences of the Type I_{FB} faulty SM and the Type $\mathrm{IV}_{\mathrm{FB}}$ faulty SM both remain at 1 during Part IV, which are consistent with the previous analysis in Section V-B. As shown in Fig. 28(d), $N_{\mathrm{FB\text{-}sw1\text{-}sum}}$ increases continuously and eventually exceeds $N_{\mathrm{FB\text{-}1th}}$. From the zoom-in figure of Fig. 28(d), $N_{\mathrm{FB\text{-}1}}$ equals 2 when the threshold is exceeded, which indicates that two faulty SMs are identified through the diagnostic method. As shown in Fig. 28(e) and (f), $N_{\mathrm{FB\text{-}FN1}}$ is 1, $N_{\mathrm{FB\text{-}FN2}}$ is 3, $N_{\mathrm{FB\text{-}FT1}}$ is 5, and $N_{\mathrm{FB\text{-}FT2}}$ is 5, which represent the sequence numbers and the faulty types of two faulty SMs correctly. The diagnosis takes 0.4 ms. It should be noted that the proposed diagnostic strategy cannot identify whether they are Type I_{FB} faults or Type $\mathrm{IV}_{\mathrm{FB}}$ faults because both these two faults share the same switching sequence characteristics in Part IV. Based on the above analysis, the proposed diagnostic strategy can diagnose Type I_{FB} fault and Type $\mathrm{IV}_{\mathrm{FB}}$ fault correctly in Part IV.

8) Experiment IV. B: Experimental waveforms of Experiment IV. B are shown in Fig. 29. As shown in Fig. 29(a). the Type I_{HB} fault occurs during Part IV. Therefore, the Type I_{HB} fault can exhibit fault characteristics immediately. As shown in Fig. 29(b), the switching sequence of the Type I_{HB} faulty

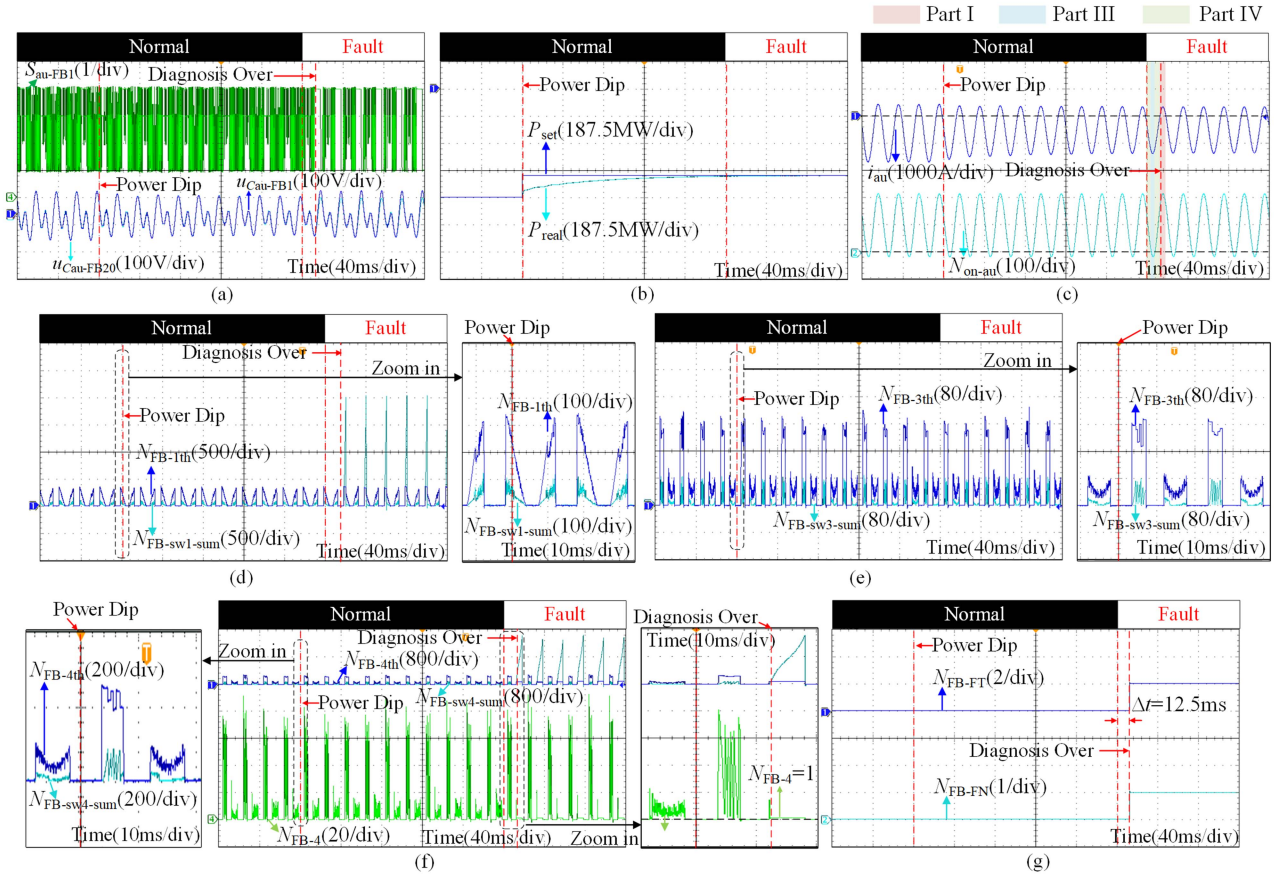

Fig. 30. Experimental waveforms under load change. (a) SM capacitor voltage and switching sequence. (b) Set active power and real active power. (c) Arm current and number of inserted SMs. (d) Relevant variables in the diagnostic method of identifying the FBSM whose $S_{\mathrm{FB}i}$ remains at 1. (e) Relevant variables in the diagnostic method of identifying the FBSM whose $S_{\mathrm{FB}i}$ remains at 3. (f) Relevant variables in the diagnostic method of identifying the FBSM whose $S_{\mathrm{FB}i}$ remains at 4. (g) Type and sequence number of faulty SM.

SM remains at 1 during Part IV, which is consistent with the previous analysis in Section V-B. Therefore, the faulty SM can be diagnosed by the diagnostic method of identifying the HBSM whose $S_{\mathrm{HB}i}$ remains at 1 during Part IV. As shown in Fig. 29(d), $N_{\mathrm{HB\text{-}sw1\text{-}sum}}$ increases continuously and eventually exceeds $N_{\mathrm{HB\text{-}1th}}$. From the zoom-in figure of Fig. 29(d), $N_{\mathrm{HB\text{-}1}}$ equals 1 when the threshold is exceeded, which indicates that a Type $\mathrm{I_{HB}}$ faulty SM is identified through the diagnostic method. As shown in Fig. 29(c), $N_{\mathrm{HB\text{-}FT}}$ is 1 and $N_{\mathrm{HB\text{-}FN}}$ is 1, which represents the sequence number and the faulty type of the faulty SM correctly. The diagnosis takes 0.3 ms. Based on the above analysis, the proposed diagnostic strategy can diagnose Type $\mathrm{I_{HB}}$ fault correctly in Part IV.

C. Effectiveness of the Proposed Diagnostic Strategy in HBMMCs and FBMMCs

Based on the verification of Experiment I. A, Experiment I. B, Experiment I. C, Experiment IV. A, and Experiment IV. B, it is clear that the diagnostic targets of Part I and Part IV contain all six types of IGBT OCFs. Therefore, the proposed diagnostic strategy can diagnose two types of IGBT OCFs in the HBSM and four types of IGBT OCFs in the FBSM. Since HBMMCs, FBMMCs and HMMCs have the same operating principles during these two parts [4], [10], the proposed diagnostic strategy can still work effectively in both HBMMCs and FBMMCs.

D. Verification of the Performance of the Proposed Diagnostic Strategy Under Load Change

To verify the performance of the proposed diagnostic strategy under load change, the experiment under load change is conducted, whose experimental waveforms are shown in Fig. 30. To imitate load change, the active power dips from 1.0 to 0.8 p.u. at t_1 [14], [24]. It is worth noting that the diagnostic threshold remains unchanged during load change. Since the diagnostic principles of the HBSM and the FBSM are similar, taking the FBSM as an example for simplicity.

As shown in Fig. 30(a), the capacitor voltages of normal FBSMs are still well-balanced during load change. Therefore, the switching sequence of the normal FBSM is still in dynamic change as shown in Fig. 30(a). As shown in Fig. 30(b), the active power dips from 1.0 to 0.8 p.u. at t_1. The arm current of upper arm in phase A and the number of inserted SMs of upper arm in phase A are shown in Fig. 30(c). As shown in Fig. 30(d)–(f), there are no thresholds that are exceeded in their

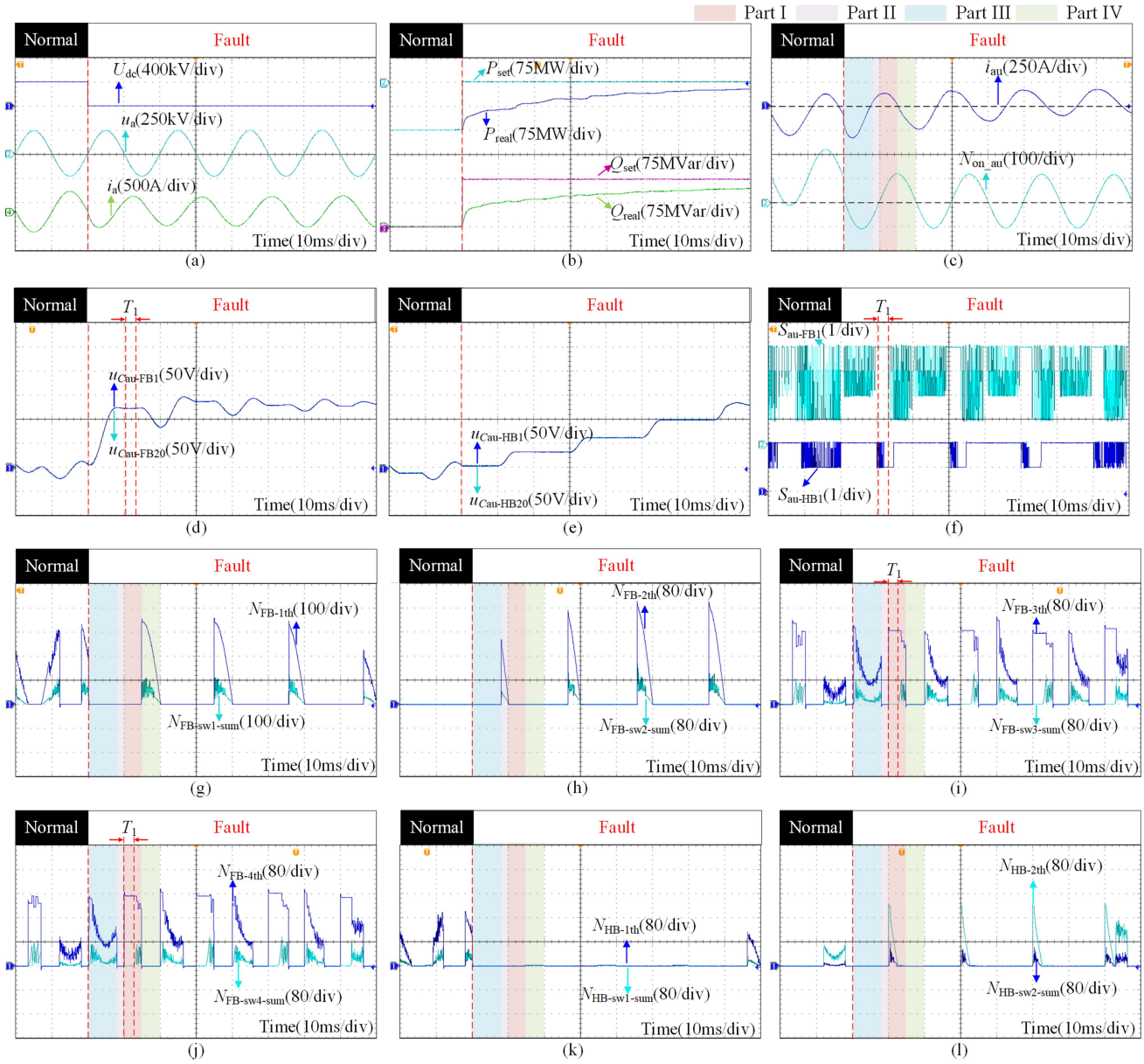

Fig. 31. Experimental waveforms under DC faults. (a) DC voltage, output voltage and output current. (b) Set active power, real active power, set reactive power and real reactive power. (c) Arm current and number of inserted SMs. (d) HBSM capacitor voltages. (e) FBSM capacitor voltages. (f) SM switching sequences. (g) Relevant variables in the diagnostic method of identifying the FBSM whose $S_{\mathrm{FB}i}$ remains at 1. (h) Relevant variables in the diagnostic method of identifying the FBSM whose $S_{\mathrm{FB}i}$ remains at 2. (i) Relevant variables in the diagnostic method of identifying the FBSM whose $S_{\mathrm{FB}i}$ remains at 3. (j) Relevant variables in the diagnostic method of identifying the FBSM whose $S_{\mathrm{FB}i}$ remains at 4. (k) Relevant variables in the diagnostic method of identifying the HBSM whose $S_{\mathrm{HB}i}$ remains at 1. (l) Relevant variables in the diagnostic method of identifying the HBSM whose $S_{\mathrm{HB}i}$ remains at 2.

activated parts of all diagnostic methods during load change. Therefore, it is demonstrated that the proposed diagnostic strategy does not mistake normal SMs as faulty SMs during load change.

Furthermore, a Type $\mathrm{II}_{\mathrm{FB}}$ fault is set to occur at t_2 to prove that the proposed strategy works effectively under different loads without reselecting the threshold. As shown in Fig. 30(f) and (g), the sequence number and the faulty type can be diagnosed correctly by the proposed diagnostic strategy. Since the diagnostic process is similar to that in Experiment I. A, it is not repeated here. Based on the above verification, it is demonstrated that the proposed diagnostic strategy works effectively under different loads without reselecting the threshold.

E. Verification of the Performance of the Proposed Diagnostic Strategy Under DC Faults

To verify the performance of the proposed diagnostic strategy under dc faults, the experiment under dc faults is conducted, whose experimental waveforms are shown in Fig. 31. The HMMC adopts the fault ride-through strategy proposed in [29] and operates equivalent to zero dc voltage conditions. As shown

in Fig. 31(a), the output current and output voltage still can be output normally with the ride-through strategy [4], [29]. As shown in Fig. 31(b), the P_{set} decreases to 0 and the Q_{set} increases to 150 MVar when a dc fault occurs [29]. The arm current of upper arm in the phase A and the number of inserted SMs of upper arm in the phase A are shown in Fig. 31(c). As shown in Fig. 31(d) and (e), the capacitor voltages of the same type SMs have an overall offset but still are well-balanced after dc faults, which is consistent with the analysis of Section VII-E. As a result, the switching sequences of the normal SMs with the same type still have consistent trends: all in dynamic change in most cases or all remain at a specific value in a specific case during the overall offset. For example, since the capacitor voltages of FBSMs are overall higher than those of HBSMs during time interval T_1, the inserted prioritization of the HBSMs is higher than FBSMs, so switching sequences of all FBSMs remain at 3 or 4 as shown in Fig. 31(f). As shown in Fig. 31(i) and (j), $N_{\text{FB-sw3-sum}}$ and $N_{\text{FB-sw4-sum}}$ both remain unchanged and do not exceed their respective threshold during T_1, thus the diagnostic methods do not mistake the normal SM as the faulty SM. As shown in Fig. 31(g)–(l), there are no thresholds that are exceeded in their activated parts of all diagnostic methods after dc faults. Therefore, it is demonstrated that the proposed diagnostic strategy does not mistake normal SMs as faulty SMs during load change.

IX. Conclusion

In this article, an improved switching method is proposed that complements the missing operating modes of the existing switching method by adding a bypassed switching sequence. Compared to the existing switching method, the proposed switching method can ensure all types of IGBT OCFs exhibit fault characteristics in a more thorough way, which is beneficial for their diagnosis. Moreover, the improved switching method keeps the switching loss unchanged compared to the existing switching method. Afterward, it is indicated that the faulty SMs remain in specific switching sequences in the corresponding part while the switching sequences of normal SMs with the same type in the HMMC are all in a dynamic change in most cases or all remain at a specific value in a specific case. On this basis, a diagnostic method is proposed to identify the faulty SM with the fixed specific sequence during a period of time while the switching sequences of other SMs with the same type are dynamic. Since six types of IGBT OCFs remain at different switching sequences in specific parts, a diagnostic strategy that consists of various types of diagnostic methods is proposed. By activating the proper diagnostic methods in each part, the proposed diagnostic strategy can diagnose all six types of IGBT OCFs within 20 ms. In this sense, the proposed strategy fills the gap in the IGBT OCFs diagnosis for HMMCs. Moreover, the proposed strategy is also applicable to HBMMCs, FBMMCs and have immunity to load change and dc faults. The effectiveness of the proposed improved switching method and the improved switching method-based diagnostic strategy is successively verified by HIL experimental results.

References

[1] S. Debnath, J. Qin, B. Bahrani, M. Saeedifard, and P. Barbosa, "Operation, control, and applications of the modular multilevel converter: A review," *IEEE Trans. Power Electron.*, vol. 30, no. 1, pp. 37–53, Jan. 2015.

[2] Y. Li, Y. Wang, and B. Li, "Generalized theory of phase-shifted carrier PWM for cascaded H-bridge converters and modular multilevel converters," *IEEE J. Emerg. Sel. Topics Power Electron.*, vol. 4, no. 2, pp. 589–605, Jul. 2016.

[3] H. Li, F. Deng, Z. Zhu, J. Lin, and Q. Zhou, "Thyristor branch loop-based hybrid modular multilevel converters for DC short-circuit faults," *IEEE Trans. Power Electron.*, vol. 39, no. 11, pp. 15070–15084, Nov. 2024.

[4] R. Zeng, L. Xu, L. Yao, and B. Williams, "Design and operation of a hybrid modular multilevel converter," *IEEE Trans. Power Electron.*, vol. 30, no. 3, pp. 1137–1146, Mar. 2015.

[5] J. Hu, M. Xiang, L. Lin, M. Lu, J. Zhu, and Z. He, "Improved design and control of FBSM MMC with boosted AC voltage and reduced DC capacitance," *IEEE Ind. Electron.*, vol. 65, no. 3, pp. 1919–1930, Mar. 2018.

[6] M. Guo, Q. Hao, and L. Ding, "Improved AAVM and small-signal model of hybrid MMC considering dynamic differences between full-bridge and half-bridge submodules," *IEEE Trans. Power Electron.*, vol. 39, no. 7, pp. 8215–8228, Nov. 2024.

[7] J. Huang, K. Li, Y. Ye, and X. Wang, "Self-balanced clamp-double submodule for modular multilevel converter," *IEEE J. Emerg. Sel. Topics Power Electron.*, vol. 10, no. 6, pp. 7249–7260, Dec. 2022.

[8] J. Qin, M. Saeedifard, A. Rockhill, and R. Zou., "Hybrid design of modular multilevel converters for HVDC systems based on various submodule circuits," *IEEE Trans. Power Del.*, vol. 30, no. 1, pp. 385–394, Jun. 2015.

[9] R. Li, L. Yu, and L. Zhong, "A hybrid modular multilevel converter with reduced full-bridge submodules," *IEEE Trans. Power Del.*, vol. 35, no. 4, pp. 1342–1350, Aug. 2020.

[10] W. Lin, D. Jovcic, S. Nguefeu, and H. Saad, "Full-bridge MMC converter optimal design to HVDC operational requirements," *IEEE Trans. Power Del.*, vol. 31, no. 3, pp. 1342–1350, Jun. 2016.

[11] H. Rao et al., "Design aspects of hybrid HVDC system," *CSEE J. Power Energy Syst.*, vol. 7, no. 3, pp. 644–653, May 2021.

[12] J. Xu, P. Zhao, and C. Zhao, "Reliability analysis and redundancy configuration of MMC with hybrid submodule topologies," *IEEE Trans. Power Electron.*, vol. 31, no. 4, pp. 1876–1885, Apr. 2016.

[13] H. Jia, Y. Deng, X. Hu, Z. Deng, and X. He, "A Concurrent diagnosis method of IGBT open-circuit faults in modular multilevel converters," *IEEE J. Emerg. Sel. Topics Power Electron.*, vol. 11, no. 1, pp. 1021–1034, Feb. 2023.

[14] Y. Jin et al., "A novel detection and localization approach of open-circuit switch fault for the grid-connected modular multilevel converter," *IEEE Trans. Ind. Electron.*, vol. 70, no. 1, pp. 110–124, Apr. 2023.

[15] L. Wang, L. Zhang, Y. Xiong, and Z. Kang, "Multi-point open circuit faults diagnosis strategy of modular multilevel converter under low modulation index," *IEEE Ind. Electron.*, vol. 71, no. 7, pp. 7886–7895, Jul. 2024.

[16] F. Deng, Y. Chen, J. Dou, C. Liu, Z. Chen, and F. Blaabjerg, "Isolation forest based submodule open-circuit fault localization method for modular multilevel converters," *IEEE Trans. Ind. Electron.*, vol. 70, no. 3, pp. 3090–3102, Mar. 2023.

[17] C. Liu, F. Deng, X. Cai, Z. Wang, Z. Chen, and F. Blaabjerg, "Submodule open-circuit fault detection for modular multilevel converters under light load condition with rearranged bleeding resistor circuit," *IEEE Trans. Power Electron.*, vol. 37, no. 4, pp. 4600–4613, Apr. 2022.

[18] J. Zhang, X. Hu, S. Xu, Y. Zhang, and Z. Chen, "Fault diagnosis and monitoring of modular multilevel converter with fast response of voltage sensors," *IEEE Trans. Ind. Electron.*, vol. 67, no. 6, pp. 5071–5080, Jun. 2020.

[19] L. Tong, Y. Chen, T. Xu, and Y. Kang, "Fault diagnosis for modular multilevel converter (MMC) based on deep learning: An edge implementation using binary neural network," *IEEE J. Emerg. Sel. Topics Power Electron.*, vol. 11, no. 6, pp. 5553–5568, Jun. 2023.

[20] F. Deng, M. Jin, C. Liu, M. Liserre, and W. Chen, "Switching open-circuit fault localization strategy for MMCs using sliding-time window based features extraction algorithm," *IEEE Trans. Ind. Electron.*, vol. 68, no. 10, pp. 10193–10206, Oct. 2021.

[21] X. Hu, H. Jia, Y. Zhang, and Y. Deng, "An open-circuit faults diagnosis method for MMC based on extreme gradient boosting," *IEEE Trans. Ind. Electron.*, vol. 70, no. 6, pp. 6239–6349, Jun. 2023.

[22] W. Zhou, J. Sheng, H. Luo, W. Li, and X. He, "Detection and localization of submodule open-circuit failures for modular multilevel converters with single ring theorem," *IEEE Trans. Power Electron.*, vol. 34, no. 4, pp. 3729–3739, Apr. 2019.

[23] X. Chen, J. Liu, Z. Deng, S. Song, S. Du, and D. Wang, "A diagnosis strategy for multiple IGBT open-circuit faults of modular multilevel converters," *IEEE Trans. Power Electron.*, vol. 36, no. 1, pp. 191–203, Jan. 2021.
[24] Z. Geng, M. Han, and L. Kou, "Repetitive signal generator-based detection method for faulty arm with switch open-circuit failure in high-voltage modular multilevel converters," *IEEE Trans. Power Del.*, vol. 37, no. 5, pp. 4073–4085, Jan. 2022.
[25] K. Li, Z. Zhao, L. Yuan, S. Lu, and Y. Jiang, "Fault detection and tolerant control of open-circuit failure in MMC with full-bridge sub-modules," in *Proc. 10th IEEE Energy Convers. Congr. Expo.*, 2016, pp. 1–6.
[26] W. Zhou, H. Yang, M. Chen, W. Li, X. He, and J. Han, "Open-circuit failure and localization of full-bridge submodules for MMCs with single ring theorem," in *Proc. 10th IEEE Appl. Power Electron. Conf. Expo.*, 2019, pp. 1794–1799.
[27] C. Liu et al., "Fault localization strategy for modular multilevel converters under submodule lower switch open-circuit fault," *IEEE Trans. Power Electron.*, vol. 35, no. 5, pp. 5190–5204, May 2020.
[28] F. Deng and Z. Chen, "A control method for voltage balancing in modular multilevel converters," *IEEE Trans. Power Electron.*, vol. 29, no. 1, pp. 66–76, Jan. 2014.
[29] R. Zeng, L. Xu, L. Yao, and D. J. Morrow, "Precharging and DC fault ride-through of hybrid MMC-based HVDC systems," *IEEE Trans. Power Electron.*, vol. 30, no. 3, pp. 1298–1306, Jun. 2015.
[30] L. Camurca, T. Pereira, F. Hoffmann, and M. Liserre, "Analysis, limitations, and opportunities of modular multilevel converter-based architectures in fast charging stations infrastructures," *IEEE Trans. Power Electron.*, vol. 37, no. 9, pp. 10747–10760, Sep. 2022.

Hong Wu (Student Member, IEEE) received the B.S. degree in electrical engineering from the Dalian University of Technology, Dalian, China, in 2021. He is currently working toward the Ph.D. degree in electricial engineering with Xi'an Jiaotong University, Xi'an, China.

His research interests include control and reliability improvement of modular multilevel converters.

Yue Wang (Senior Member, IEEE) received the B.S. degree from Xi'an Jiaotong University, Xi'an, China, in 1993, the M.S. degree from Beijing Jiaotong University, Beijing, China, in 1999, and the Ph.D. degree from Xi'an Jiaotong University, in 2003, all in electrical engineering.

From 1993 to 1996, he was an Electrical Engineer with Xi'an Power Electronics Technology Research Institute. He is currently a Full Professor with the School of Electrical Engineering, Xi'an Jiaotong University. His research interests include wireless power transfer, active power filters, multilevel converters, and HVdc.

Yi Liu (Student Member, IEEE) received the B.S. degree in electrical engineering and automation from Jilin University, Changchun, China, in 2021. He is currently working toward the Ph.D. degree in electricial engineering with Xi'an Jiaotong University, Xi'an, China.

His research interests include sequence impedance modeling, control and stability analysis of power electronic in power systems.

Yonghui Liu (Member, IEEE) received the B.S. degree from the Harbin Institute of Technology, Harbin, China, in 2013, the M.S. degree from Xi'an Jiaotong University, Xi'an, China, in 2016, and the dual Ph.D. degree from Xi'an Jiaotong University and Hong Kong Polytechnic University, Hong Kong, in 2023, respectively, all in electrical engineering.

She is currently an Assistant Professor with Xi'an Jiaotong University. Her research interests include modeling and control of grid-forming converters, renewable energy integration, and VSC-HVDC.

Yufei Li (Senior Member, IEEE) received the B.S. and Ph.D. degrees in electrical engineering from Xi'an Jiaotong University (XJTU), Xi'an, China, in 2009 and 2016, respectively.

He was given the exam exemption for outstanding undergraduates to pursue the M.S. degree in 2009, and pivoted to directly pursue the Ph.D. degree in 2011. From 2019 to 2021, he was a Postdoctoral Fellow with the Department of Electrical Engineering, University of Arkansas, Fayetteville, AR, USA. From 2021 to 2023, he was an Associate Research Scholar with the Department of Electrical and Computer Engineering and Andlinger Center for Energy and the Environment, Princeton University, Princeton, NJ, USA. Since 2023, he has been with the School of Electrical Engineering, Xi'an Jiaotong University, where he is currently an Associate Professor. His research interests include wide bandgap power device applications, advanced power conversion for grid integration, topology and control of high-power power conversion systems, artificial intelligence and machine learning methods for power electronics systems.

Dr. Li was selected for the 2023 Outstanding Reviewer Awards for IEEE TRANSACTIONS ON POWER ELECTRONICS.